Published in final edited form as:
J Neurosci. 2010 July 28; 30(30): 10112–10126. doi:10.1523/JNEUROSCI.6344-09.2010.

Ric-3 promotes α7 nicotinic receptor assembly and trafficking through the ER sub-compartment of dendrites

John K. Alexander,
Department of Neurobiology, The University of Chicago, Chicago, IL, 60637, USA

Daphna Sagher,
Department of Neurobiology, The University of Chicago, Chicago, IL, 60637, USA

Arcadius V. Krivoshein,
Department of Molecular Biology and Genetics, Cornell University, Ithaca, New York, 14853, USA

Manuel Criado,
Instituto de Neurociencias de Alicante, Universidad Miguel Hernández-CSIC, Sant Joan d'Alacant, Alicante, Spain

Gregory Jefford, and
Department of Neurobiology, The University of Chicago, Chicago, IL, 60637, USA

William N. Green
Department of Neurobiology, The University of Chicago, Chicago, IL, 60637, USA

Abstract

The function of Ric-3, which is required for nicotinic acetylcholine receptor (nAChR) expression in *C. elegans*, is unclear. Here we found that Ric-3 can promote or inhibit cell-surface delivery of α-Bungarotoxin-binding nAChRs (BgtRs) composed of α7 subunits. At low levels, Ric-3 promoted BgtR assembly, endoplasmic reticulum (ER) release and cell-surface delivery without trafficking from the ER. At high Ric-3 levels, Ric-3 suppressed BgtR surface delivery, but not its assembly, and BgtRs were retained in the ER or in Ric-3-containing aggregates. In PC12 cells, native BgtRs trafficked to the cell surface from the ER where low levels of endogenous Ric-3 were observed. In cultured neurons, native Ric-3 levels were higher than in PC12 cells, and Ric-3 and α7 subunits were found in somata and dendrites, but not axons, of inhibitory interneurons. Ric-3 trafficked with α7 subunits in rapidly moving vesicles to dendrites where it was restricted to the ER sub-compartment. We conclude that Ric-3 has two potential functions. At low levels, Ric-3 interactions are short–lived and promote BgtR assembly and ER release. At higher levels, Ric-3 interactions are longer–lived and mediate ER retention. In neurons, Ric-3 ER retention appears to promote transport within the dendritic ER sub-compartment, thereby restricting α7 trafficking to dendrites and preventing axonal transport.

Keywords

Ric-3; BgtR; bungarotoxin; nicotinic acetylcholine receptor; α7; ER retention; dendrite

Corresponding Author: William N. Green, wgreen@uchicago.edu.

Introduction

Nicotinic acetylcholine receptors (nAChRs) are members of the cys-loop family of neurotransmitter-gated ion channels (Karlin and Akabas, 1995; Albuquerque et al., 2009). The first neuronal nAChR subtype was identified by its high-affinity α-bungarotoxin (Bgt) binding (Betz et al., 1982; Conti-Tronconi et al., 1985; Kemp et al., 1985; Whiting and Lindstrom, 1987)Bgt-binding nAChRs (BgtRs) are found on neurons throughout the nervous system at presynaptic terminals, at postsynaptic sites and extrasynaptic sites and on other non-neuronal cell types (Wang et al., 2003) (Grando et al., 1996; Sekhon et al., 1999). BgtRs are nAChRs composed of a single subunit subtype, α7 subunits (Chen and Patrick, 1997; Rangwala et al., 1997; Drisdel and Green, 2000). Additionally, BgtRs are assembled only in certain cell types (Blumenthal et al., 1997; Cooper and Millar, 1997; Rangwala et al., 1997) suggesting that they require cell-specific conditions to properly fold and assemble. Indeed, the palmitoylation of α7 subunits occurs during BgtR assembly in the ER and is absent in cells unable to assemble BgtRs (Drisdel et al., 2004). However, cells unable to assemble BgtRs can palmitoylate other proteins indicating that additional factors help regulate BgtR assembly.

Ric-3 was first identified in *C. elegans* (Nguyen et al., 1995; Miller et al., 1996) and is required for nAChR biogenesis and cell-surface expression (Halevi et al., 2002). With reports that Ric-3 promoted (Cheng et al., 2005; Lansdell et al., 2005) or inhibited (Halevi et al., 2003; Castillo et al., 2005) 5HT3 receptors and α4β2 nAChR surface expression, there is uncertainty about how Ric-3 affects these receptors. There is also no consensus about the sub-cellular localization of Ric-3 with most studies finding Ric-3 at ER membranes (Castillo et al., 2005; Cheng et al., 2005; Wang et al., 2009) but also at the cell surface (Williams et al., 2005) and Golgi apparatus (Castillo et al., 2005). Studies showing that Ric-3 and receptor subunits co-immunoprecipitate (Cheng et al., 2005; Lansdell et al., 2005; Williams et al., 2005; Wang et al., 2009) suggest that Ric-3 chaperones receptor assembly in the ER through long-lived interactions with the subunits.

Here, we find that Ric-3 activity depended on its expression levels. At low levels, it acted in the ER to promote α7 subunit assembly and surface delivery. At higher levels, Ric-3 suppressed α7 surface delivery and retained it in the ER. In PC12 cells, endogenous Ric-3 expression levels are low and appear to promote α7 subunit assembly and surface delivery. In cultured neurons, Ric-3 levels are higher than in PC12 cells and Ric-3 is found in the ER of somata and the ER sub-compartment of dendrites, where it co-localizes with α7 subunits. Our results indicate that at low levels short-lived interactions with α7 subunits predominated and Ric-3 facilitated BgtR assembly, ER-release and cell-surface delivery. At higher levels, longer-lived interactions predominated that retained BgtRs in the ER. In neurons, Ric-3 retained α7 subunits in the ER sub-compartment of dendrites where they were transported together in vesicles within the ER sub-compartment. In this way, Ric-3 long-lived interactions preferentially traffic α7 subunits synthesized in the soma to dendrites instead of axons.

Methods

Cell Culture and Constructs

The human embryonic kidney (HEK) cell line stably transfected with the large T antigen (tSA201 cells) was from Dr. J. Kyle (University of Chicago, Chicago, IL) and maintained in DMEM supplemented with 10% calf serum (Hyclone, Logan, UT). The PC12 cell subclone, PC12 N21 or PC12-C cells (Blumenthal et al., 1997), was from Dr. Richard Burry (Ohio State University, Columbus, OH). The cells were cultured in DMEM containing 5% heat-inactivated horse serum and 10% fetal bovine serum (Hyclone). Primary hippocampal neurons were prepared in the University of Chicago Neuronal Tissue Core using Sprague-Dawley rats at embryonic day 18 (E18). As previously described (Marks et al., 2000), hippocampi from day

18 embryos were separated from the diencephalon, dissected free of meninges, and diced. Hippocampi were digested in 0.1% (wt/vol) trypsin and 0.015% DNAse. After dissociation by trituration, cells were counted, suspended in plating medium consisting of Neuralbasal-A supplemented with 2% B-27 (both from Gibco-Invitrogen Corp), 0.5 mM L-glutamine and 0.025 mM L-glutamate. Cells were plated on poly L-lysine-coated 12-mm cover slips at a density of 8×10^4 cells/cm^2. For the live imaging studies, E18 hippocampi were purchased from BrainBits LLC, (Springfeild, IL) and prepared per manufucaturer's instructions. All cultures were maintained at 37°C and 5% CO_2. Chick α7 and chick/mouse α7/5HT3A subunit plasmids were cloned into pMT3 (Rakhilin et al., 1999) and the human Ric-3 cDNA in pcDNA3 was a gift from Dr. Treinin. The fusion of cyan fluorescent protein (CFP) to the N-terminus of Ric-3 was generated by subcloning Ric-3 into the pECFP-C1 vector (Clontech). An EcoRI site was inserted just 5' to the start codon of Ric-3 using the Quikchange site directed mutagenesis kit (Qiagen). The resulting Ric-3 cDNA was inserted between the EcoRI and SmaI sites of pECFP-C1. The FLAG epitope (DYKDDDDK) was inserted just after the start codon of Ric-3 using the extension overlap method (Ho et al., 1989). The ER marker, DsRed-ER, was purchased from Clontech.

Cell Transfections

HEK cell transient transfections (5 μg α7 or α7/5HT3A plasmid, varying amounts of Ric-3 plasmid) were performed using the calcium phosphate method (Eertmoed et al., 1998). The total plasmid per transfection was 10 μg for a 6-cm plate (p60), with levels adjusted with the pcDNA3 plasmid. The pMT3 and pcDNA3 plasmids without cDNA insert were used for control transfections without cDNAs (sham). Neuronal transfections were carried out on 14–18 days in-vitro cultures using Lipofectamine2000 (Invitrogen) according to manufacturer's instructions. Briefly, plasmid and Lipofectamine2000 reagent were mixed in a one-to-one ratio and complexed in Neuralbasal-A media for 30 minutes. The complex was drop-wise added to neuronal cultures in 12-well plates and returned to the incubator for 24 hours prior to processing for immunofluorescence.

^{125}I-Bgt Binding Assays

Intact cells were incubated with ^{125}I-Bgt for 2 hours at room temperature in PBS with 1 mM EDTA and 10 mM HEPES pH 7.4. For cells expressing α7, 4 nM ^{125}I-Bgt (140–170 cpm/fmol; PerkinElmer) was used. For cells expressing α7/5HT3A, ^{125}I-Bgt was cut 1 to 9 with cold Bgt and 100 nM total Bgt was used to avoid depletion of the Bgt. Intact cells were collected, washed three times with PBS and counted with a LKB-Wallac (Gaithersburg, MD) 1470 automatic gamma counter. Cells were lysed in Lysis Buffer with Triton (LBT): 150 mM NaCl, 5mM EDTA, 50 mM Tris, pH 7.4, 1% Triton X-100 supplemented with protease inhibitors (PIs): 2 mM phenylmethylsulfonyl fluoride, 10 μg/ml each of chymostatin, pepstatin, leupeptin, and tosyl-lysine chloromethylketone, and 50 nM N-ethylmaleimide (NEM). Lysates were centrifuged at 16000×g and supernatants incubated with 50 μl of concanavalin A-sepharose slurry (ConA, Sigma Aldrich) for 3 hours at room temperature, which quantitatively precipitates all (surface plus internal) BgtRs. To measure internal ^{125}I-Bgt binding, ^{125}I-Bgt binding to cell-surface BgtRs was estimated by ConA-sepharose precipitation after ^{125}I-Bgt binding to intact cells and solubilization. ^{125}I-Bgt binding to all BgtRs (surface plus internal) was estimated by incubating the ConA-sepharose precipitated BgtRs again with ^{125}I-Bgt for 2 hours at room temperature. ^{125}I-Bgt binding to internal BgtRs was calculated by subtracting the cell-surface from the total ^{125}I-Bgt binding. A final estimate of internal ^{125}I-Bgt binding, adjusted for the loss with ConA pulldown, was made by multiplying by the ratio, surface ^{125}I-Bgt binding to intact cells: surface ^{125}I-Bgt binding from ConA pulldown. We determined protein concentrations (mg/ml) from an aliquot of supernatant using the BCA protein assay (Pierce).

Western Blots

Cultures were rinsed 3 times with PBS and lysed in LBT with PIs. Insoluble material was pelleted via centrifugation at 16000×g and the supernatant transferred to a new tube. Protein concentration was determined by the BCA protein assay (Pierce), and all samples were diluted to 1 mg/ml. Samples were then reduced with 50 mM TCEP and alkylated with 10 mM NEM for 30 minutes, then denatured for SDS-PAGE with 5x Laemmli sample buffer. Each lane was loaded with 200 μg total protein, which was the maximum amount of protein that did not distort SDS-PAGE and was analyzed on a 8% SDS-PAGE gel which was transferred to a PVDF membrane and probed with the following antibodies: rabbit anti-actin (1:1000, Sigma), chicken anti-Ric3 (1:100 (Castelan et al., 2008)), or mouse anti-FLAG-M2 (1:1000, Sigma), goat anti-α7 (1:100, Santa Cruz), mouse anti-FLAG-M2 (1:1000, Sigma) overnight at 4°C. Membranes were washed and probed with appropriate fluorescent secondary antibodies (Jackson Immunocytochemical or Molecular Probes, Invitrogen) for 1 hour at room temperature. Fluorescence was detected using a Biorad Molecular Imager Pharos-FX which allowed for quantification using ImageJ (Rasband, 1997–2009).

Flow Cytometry

For surface BgtR labeling, transiently transfected cultures were incubated with 100 nM Alexa-647-Bgt (Molecular Probes, Invitrogen) for 1 hour at room temperature. The cells were washed 2x with PBS, incubated in PBS with 10 mM HEPES pH 7.4 and 1 mM EDTA for 15 minutes to gently lift the cells off the plate. Sterile Fluorescence Assisted Cell Sorting (FACS) was performed with the BD FACSAria using a 405 nm Violet and 633 Red Diode laser. Non-specific Alexa-647-Bgt binding or autofluorescence was determined by measuring the fluorescence from sham transfected cultures. Sorting thresholds (gates) were set to collect cells with fluorescence intensities above those measured from sham transfected cells as illustrated in Fig. 2. Collected cells were gently centrifuged at 100×g for 5 minutes and resuspended in regular culture media. 1×10^5 cells were seeded onto collagen coated coverslips (10 μg/ml) and allowed to adhere for 12 hours. Cultures were then processed for immunocytochemistry as described below. Analysis of FACS data was performed using the FlowJo software.

Whole-Cell Patch Clamp Recording

Sterile sorted cells were shipped live via priority overnight delivery to collaborators at Cornell University. The whole-cell currents were recorded with use of an Axopatch 200A integrating patch clamp amplifier and Clampex 9 data acquisition software (both from Axon Instruments, Foster City, CA) as described by Hamill et al. (Hamill et al., 1981). The composition of the buffer in the recording electrode was 140-mM KCl, 2-mM MgCl2, 1 mM CaCl2, 11 mM ethylene glycol-bis(β-aminoethyl ether)-N, N, N′, *N*′-tetraacetic acid (EGTA), and 25 mM N-2-hydroxyethylpiperazine- *N*′-2-ethanesulfonic acid (HEPES), adjusted to pH 7.4 with KOH. The composition of the extracellular (bath) buffer was 145 mM NaCl, 3-mM KCl, 2 mM MgCl2, 1 mM CaCl2, and 25 mM HEPES, adjusted to pH 7.4 with NaOH. Recording electrodes were pulled from borosilicate glass capillaries on a PIP5 two-stage vertical pipette puller (HEKA Elektronik, Lambrecht / Pfalz, Germany), and the electrode resistance was typically 2–3 MΩ. The series resistance was typically 3–5 MΩ, and was up to 70% compensated electronically. All measurements were carried out at room temperature (22–24 °C) and a membrane potential of − 60 mV. 1 mM ACh-Cl dissolved in the extracellular buffer was applied for 0.2 s using cell-flow technique (Udgaonkar and Hess, 1987). Data were low-pass filtered at 2 kHz (4-pole Bessel filter) and digitized at 5 kHz.

Immunocytochemistry

For cell surface BgtR labeling, live cultures were incubated with 100 nM fluorescent Bgt (Molecular Probes, Invitrogen) for 30 minutes at 37°C. To block surface BgtRs for labeling of

internal BgtRs, live cultures were incubated with 100 nM unlabeled Bgt for 30 min at 37°C. Cultures were washed 3 times with culture medium then processed as follows. Cells were fixed in 2% paraformaldehyde with 75 mM Lysine and 10 mM periodate in PBS (PLP) for 10 minutes, quenched with 100mM Glycine for 10 minutes, and permeabilzed with 0.5% Triton X-100 for 10 minutes. Blocking of non-specific sites was performed with 5% Normal Donkey Serum (NDS) and 0.1% fish gelatin in PBS for 1 hour prior to incubating with primary antibodies in blocking solution overnight at 4°C. Antibodies and dilutions used were: Anti-PDI at 1:2500 (ABR), anti-GM130 at 1:300 (BD Transduction Labs), fluorescent bungarotoxin (100 nM, Molecular Probes), anti-α7 (1:100, Santa Cruz), anti-Ric-3 (1:100, (Castelan et al., 2008)), anti-MAP2 (1:1000, Cell Signaling Technology), anti-NFH (1:1000, Aves Labs), anti-GAD (1:1000, Chemicon). Cells were then incubated in appropriate secondary antibodies as described in figure legends (1:1000) for 1 hour at room temperature. In some cases, nuclei were labeled with Hoechst dye for 5 minutes. Cells were mounted in ProLong gold and allowed to cure for 24 hours prior to imaging on either the Olympus DSU spinning disk or Leica SP-5 scanning laser confocal microscope (Integrated Microscopy Facility, University of Chicago). To facilitate quantitative fluorescence measurements, care was taken so that microscope settings were set below saturating fluorescence intensities. To estimate background fluorescence samples were prepared without primary antibody or, in the case of Bgt, by including 1 mM nicotine for 5 minutes before and during FL-Bgt labeling in the presence of 1 mM nicotine.

Image Analysis

In supplemental Fig. 2, sorted HEK cells were judged as containing CFP-Ric-3 aggregates if the cells contained one or more large aggregates or two or more smaller aggregates. To estimate the amount of Ric-3 or Fl-Bgt labeling in PC12 cells and neurons preference was given to isolated cells. Each cell was circled using ImageJ software and the total fluorescence for each slice of a confocal stack was estimated and summed. To estimate the intensity of Fl-Bgt puncta, we measured the fluorescence intensity of n puncta, averaged the data and compared it to fluorescence intensity measurements of a same size region within 1 μm of the puncta. To estimate the size of Fl-Bgt puncta, the number of pixels through the center of the puncta was determined, and the corresponding pixel size used to calculate the diameter (0.16 μm per pixel at 100x). In Fig. 5G, sorted HEK cells were judged as containing Fl-Bgt puncta if they contained 4 or more Fl-Bgt puncta. In all cases, background fluorescence was determined by performing an identical analysis on cells labeled in the absence of primary antibody or, for Fl-Bgt imaging, labeled in the presence of nicotine as described above. When necessary, randomly sampled images were acquired by choosing fields of view using DIC.

Degree of Colocalization Estimations

For colocalization analysis of confocal stacks, we used the ImageJ Intensity Correlation Analysis plug-in (Li et al., 2004). Images were first deconvolved using the Huygens Pro deconvolution software (SVI Inc). Individual cells were carefully outlined (including dendrites if analyzing neurons) and cropped, pixel intensities normalized to maximum intensity for each fluorophore and the resulting confocal stack was then processed by the Intensity Correlation Analysis plug-in. The frequency scatter plot generated is used to illustrate the extent of colocalization and the Mander's overlap coefficient as was determined from at least 10 cells used to test for significance.

Statistical Analysis

Results are expressed as mean ± standard error of the mean (SEM) of *n* samples. Statistical significance was assessed by a two-tailed Student's t-test or ANOVA as appropriate using Microsoft Excel.

Results

Ric-3 promotes and inhibits BgtR cell-surface delivery

To investigate the effects of Ric-3 on BgtR formation in more detail, we varied the amount of human Ric-3 plasmid transfected with either the α7 subunit or a chimeric subunit composed of the N-terminal half of α7 and the C-terminal half of 5HT3A subunits (α7/5HT3 subunits) (Fig. 1). Unlike the α7 subunit, the α7/5HT3 subunit does not require Ric-3 to form BgtRs in HEK cells (Eisele et al., 1993;Rangwala et al., 1997). We compared the effects of Ric-3 on BgtR formation and cell-surface expression by measuring intracellular and surface ^{125}I-Bgt binding to α7 (Fig. 1A) or α7/5HT3 BgtRs (Fig. 1B). Intracellular ^{125}I-Bgt binding to α7 BgtRs increased 5-fold over the whole range of transfected Ric-3 plasmid. In contrast, cell-surface expression peaked with a 40-fold increase at much lower levels of Ric-3 plasmid and declined to a 12-fold increase at higher levels of Ric-3 plasmid. Levels of intracellular ^{125}I-Bgt binding to α7/5HT3 chimeric BgtRs were independent of transfected Ric-3 plasmid and cell-surface expression was unaffected at lower levels of Ric-3 plasmid and showed a steep decline at the higher levels of Ric-3 plasmid (Fig. 1B). Ric-3 protein levels were assayed by immunoblots using FLAG-tagged Ric-3 (Fig. 1C) and there was no difference between FLAG-tagged and untagged Ric-3 with respect to how varying Ric-3 plasmid affected BgtR cell-surface expression (data not shown). Ric-3 levels rose linearly with increasing transfected plasmid amounts in the range in which FLAG-Ric-3 protein was detectable (corresponding to 0.01 to 2.5 μg Ric-3 plasmid). Ric-3 protein levels are a linear function of transfected plasmid below 2.5 μg, whereas above 2.5 μg transfected plasmid, Ric-3 protein levels saturated. We examined a generic membrane protein, CD8α, and found its surface expression was unaltered by high Ric-3 levels (supplemental Fig. 1), which indicates that the decline in surface ^{125}I-Bgt binding we observed at high Ric-3 levels was specific to α7 and α7/5HT3 BgtRs and not a general effect of Ric-3 on membrane protein trafficking.

We have previously observed that Bgt binding sites form on α7 and α7/5HT3 chimeric BgtRs during subunit assembly in the ER and that intracellular ^{125}I-Bgt binding is a measure of the amount of newly assembled BgtRs prior to surface insertion (Rakhilin et al., 1999; Drisdel et al., 2004). The increased number of intracellular α7 BgtRs with Ric-3 levels (Fig. 1A), thus, indicates that Ric-3 enhances Bgt site formation and α7 BgtR assembly in the ER. There was no effect of varying Ric-3 levels on the levels of α7 subunit protein, which remained constant over the range of Ric-3 tested (data not shown). In contrast to α7 BgtRs, there was no change in intracellular α7/5HT3 BgtRs with Ric-3 levels (Fig. 1B) from which we conclude that Ric-3 has little to no effect on α7/5HT3 BgtR assembly. The lack of a Ric-3 effect on α7/5HT3 Bgt site formation could be explained if the levels of α7/5HT3 BgtRs assembled were already at saturating levels in the absence of Ric-3. This is consistent with the observation that ~50% of the total α7/5HT3 BgtRs are expressed on the cell surface in the absence of Ric-3 and that at peak surface expression of α7 BgtRs with Ric-3 co-expression, 45% of the total α7 BgtRs are also expressed on the cell surface (Fig. 1D) suggesting that the cell is at its maximum capacity for expressing surface BgtRs in relation to the total number available.

Ric-3 appears to have two separate actions on α7 subunits. The first effect is observed at low Ric-3 levels (0 to 0.1 μg plasmid) where there is an increase in subunit assembly into BgtRs as well as increased α7 BgtR forward trafficking. This effect is caused by increased BgtR assembly that, in turn, increased the rate of the forward trafficking. These effects occur at such low levels of Ric-3 plasmid (Fig. 1A) and protein (Fig. 1D) that the interactions between Ric-3 and α7 subunits are very far from stoichiometric. For such a small amount of Ric-3 to alter much larger amounts of α7 subunits, the data indicates that the interaction between Ric-3 and α7 subunits causing these effects is short lived. The third effect is observed at higher Ric-3 levels (0.1 to 5.0 μg plasmid), where Ric-3 blocked BgtR insertion at the cell surface for α7 and α7/5HT3 BgtRs. Because Ric-3 only inhibited cell-surface and not intracellular BgtR

levels, Ric-3 appears to block BgtR forward trafficking to the cell surface without altering its actions on BgtR assembly. Because these effects occur when Ric-3 and subunit plasmid levels are approximately equal, interactions between Ric-3 and the subunits may be much much longer lived and may act to sterically retain the subunits within a compartment in the cells. A longer-lived interaction between Ric-3 and the subunits is indicated by our ability (data not shown) and others (Cheng et al., 2005;Williams et al., 2005;Wang et al., 2009) to co-immunoprecipitate Ric-3 and the subunits at the higher Ric-3 levels.

Ric-3 alters BgtR cellular distribution and localization

To further address how Ric-3 affects BgtR expression, we examined their distribution at the single-cell level using fluorescence microscopy. From the outset, we found that the cell-to-cell variations resulting from transient transfection of the constructs made it difficult to analyze the experiments. Also, antibodies (Abs) generated against the Ric-3 C-terminal cytoplasmic domain (Castelan et al., 2008) could not reliably detect Ric-3 transfected with 0.01 μg plasmid or less. To address these problems, we generated a fluorescent Ric-3 construct tagged with cyan fluorescent protein (CFP) at its N-terminus (CFP-Ric-3) and used fluorescence-based flow cytometry to select cells for immunofluorescence microscopy. This strategy isolated more uniform populations of cells in terms of surface BgtR and Ric-3 expression. To assay BgtRs on the cell surface with cell sorting, BgtRs were stained with fluorescently labeled Bgt (Fl-Bgt). With the addition of the CFP tag, Ric-3 reduced α7 subunit synthesis when transfected higher then at 0.1 μg plasmid (data not shown). We avoided reduced α7 subunit synthesis by using a mixture of CFP-tagged (no more than 0.1 μg) and untagged Ric-3 for transfections with Ric-3 plasmid levels greater than 0.1 μg (data not shown). The CFP-tagged Ric-3 had the same cellular distribution as the untagged Ric-3 when co-transfected at both low and high levels of total Ric-3 (supplemental Fig. 2A).

We performed cell sorting on three sets of transfected cells. One set of cells was sorted from cells expressing α7 subunits and no Ric-3 (Fig. 2A–C). Results from the cell sort are displayed in Fig. 2A where each point represents single-cell fluorescence values for surface Fl-Bgt (y-axis) and, in this case CFP (x-axis). Very few cells had significant Fl-Bgt staining on the cell-surface consistent with the ^{125}I-Bgt staining of the cells (Fig. 1A). This result was verified using immunofluorescence microscopy on the sorted cells (Fig. 2B). Because of a lack of Fl-Bgt staining, cells were co-transfected with a CFP plasmid to help select for cells that contain α7 subunits without Fl-Bgt staining. There was a high degree of α7 and CFP co-expression (92.3% ± 0.3%, n=3 fields of view, 119 cells total) in cultures transfected with α7 and CFP plasmid (Fig. 2B,C). Another set of cells was sorted from cells expressing α7 subunits and low levels of Ric-3 (Fig. 2D–F). As expected, large numbers of these cells were stained for Fl-Bgt (89.5% ± 1.5%, n=3 fields of view, 137 cells total) yet most cells lacked levels of CFP-Ric-3 fluorescence detectable by the flow cytometer (Fig. 2D). Because so few cells with α7 alone expressed detectable levels of surface BgtR, the cells co-transfected with CFP-Ric-3 exhibiting surface Bgt staining must express some CFP-Ric-3 even though most of them (95%) had CFP fluorescence undetectable by the flow cytometer. CFP-Ric-3 fluorescence was detectable in a higher percentage of the cells using a fluorescent scanning microscope (19.5% ± 3.1% of n=3 fields of view, 190 cells total) as shown in Figs. 2E and F. Displayed in Fig. 2E are two cells that are surface stained with Fl-Bgt. One cell was positive for CFP-Ric-3 fluorescence and in the other cell CFP-Ric-3 fluorescence was undetectable as observed for most cells. These results provide further evidence that the Ric-3 levels that mediate α7 BgtR assembly and surface delivery are extremely low such that they are often undetectable by immunoblot (Fig. 1C), flow cytometry (Fig. 2D) or by fluorescent microscopy measurements (Fig. 2E). In the cells positive for Fl-Bgt and CFP-Ric-3 fluorescence, there was no detectable overlap of CFP-Ric-3 and surface Fl-Bgt fluorescence (e.g., Fig. 2E, inset). This finding indicated that little to no Ric-3 trafficked with α7 BgtRs to the cell-surface or that Ric-3 was rapidly internalized once

it arrived at the cell surface. In cells with detectable levels of CFP-Ric-3 fluorescence, Ric-3 was diffusely distributed throughout much of the cell with a perinuclear and reticulated pattern typical of the ER.

A final set of cells was sorted from cells expressing α7 subunits and high levels of Ric-3 (Fig. 2G–I). At high Ric-3 levels, the number of Fl-Bgt positive cells was reduced (Fig. 2G), consistent with the decrease in surface ^{125}I-Bgt binding observed at high Ric-3 levels (Fig 1A). Cells lacking surface Fl-Bgt tended to have significant CFP-Ric-3 fluorescence and we sorted for the cells that were positive for CFP-Ric-3 and lacked Fl-Bgt (boxed area in Fig. 2G). An example typical of this cell population is displayed in Figs. 2H and I. The distribution of Ric-3 and α7 subunits in these cells was different from cells with lower Ric-3 expression. In addition to a diffuse distribution of Ric-3 and α7 subunits throughout the cells, there were round aggregated structures with hollow centers (see inset in Fig. 2H). Similar aggregated structures were observed previously with heterologous expression of Ric-3 (Castillo et al., 2005; Cheng et al., 2005; Wang et al., 2009). To further analyze Ric-3's cellular distribution, we determined the number of cells with aggregates as in Figs. 2H and I, or free of aggregate as in Figs. 2E and F. We did not find any aggregates at low Ric-3 levels when cells were positive for surface Fl-Bgt staining (supplemental Fig. 2). At high Ric-3 levels, 70–80% of the Bgt positive cells had aggregates and 20–30% of the cells lacked them (supplemental Fig. 2C). Thus, aggregates of Ric-3 and α7 subunits were observed in cells with high Ric-3 levels in which BgtRs were transported to the cell surface suggesting that the aggregates alone are not totally responsible for inhibiting surface delivery of BgtRs, or, that the aggregates formed subsequent to surface delivery of BgtRs. In cells with no significant Bgt staining (supplemental Fig. 2D), Ric-3 aggregates were observed at all levels of Ric-3 expression together with a diffuse distribution of Ric-3. Ric-3 aggregates were even observed at the lower levels of Ric-3 expression suggesting that in a small population of these cells Ric-3 levels were high enough so that aggregates formed.

Ric-3 regulation of α7 BgtR function

Previous studies have found increased numbers of functional α7-containing BgtRs with the addition of Ric-3 to the cells but did not test whether the increase varied with changes in Ric-3 levels. To address this question, we performed whole-cell patch clamp recordings on sorted cells transfected with α7 and varying levels of Ric-3 plasmid (Fig. 3). Sorted cells positive for Fl-Bgt staining generally displayed rapidly desensitizing ACh-evoked currents, a feature of α7 nAChRs. An example is displayed in the inset in Fig. 3. We observed no ACh-evoked currents from cells without significant Fl-Bgt staining. As shown in Fig. 3, the frequency of observing a response (19 out of 25 cells) and mean amplitude was significantly larger for cells with low Ric-3 levels than for cells with high levels of Ric-3 (8 out of 15 cells). Cells with α7 subunits but no Ric-3 did have ACh-evoked currents, but the frequency of the responses (9 out of 16 cells) and their mean amplitude was significantly smaller than for cells at the two Ric-3 levels. From these measurements, we conclude that the number of functional receptors has the same dependence on Ric-3 levels as the number of cell-surface BgtRs as determined in Figs. 1 and 2 using ^{125}I-Bgt or Fl-Bgt.

Cellular localization of Ric-3 in the absence of α7 subunits

Contrary to a previous report (Williams et al., 2005), we did not observe co-localization between Ric-3 and surface BgtRs (Fig. 2E). Ric-3 was also reported in the Golgi complex (Castillo et al., 2005) as well as in the ER (Castillo et al., 2005; Cheng et al., 2005; Wang et al., 2009). In Fig. 4, we tested whether Ric-3, in the absence of α7 subunits, is predominantly in the ER or at other sites along the secretory pathway such as the Golgi complex. Cells with high or low Ric-3 levels and no α7 subunits were sorted using CFP-Ric-3 fluorescence to isolate a more homogenous population of cells containing different Ric-3 levels. These cells were

stained with an ER marker (protein disulfide isomerase (PDI) specific Ab), or a Golgi marker (GM-130 specific Ab). At the low Ric-3 levels, CFP-Ric-3 co-localized strongly with the ER marker and little to none with the Golgi marker (Fig. 4A). We gauged the degree of colocalization by comparing the intensities of the two fluorophores pixel by pixel in the confocal images (see supplemental Fig. 3 for details). The degree of linear correspondence between the CFP-Ric-3 fluorescence and that of the ER marker was determined (see supplemental Fig. 3) from which we obtained a Manders coefficient (Manders et al., 1992), R with values from 1 (perfect overlap) to 0 (no overlap). 86% of the CFP-Ric-3 pixels co-localized with those of the ER marker ($R = 0.66 \pm 0.1$, n=10 cells, supplemental Fig. 3B) indicating strong co-localization. In contrast, no significant co-localization between CFP-Ric-3 and the Golgi marker was found as shown by the lack of correspondence between the CFP-Ric-3 fluorescence and that of the Golgi marker (Fig. 4C). Only 2% of the CFP-Ric-3 pixels overlapped with the Golgi marker and 6% of the Golgi marker pixels overlapped with CFP-Ric-3 pixels ($R = 0.12 \pm 0.03$, n=10 cells, supplemental Fig. 3B). Thus at low Ric-3 levels, Ric-3 is predominantly localized in the ER and not in the Golgi or at the cell-surface.

At high levels of Ric-3 (Fig. 4D,E,F), the Ric-3 distribution changed and we observed aggregated structures just like when Ric-3 was co-expressed with α7 subunits (Fig. 2F,I). Together with a lack of α7 subunit aggregates in the absence of Ric-3, this finding, demonstrates that Ric-3 mediates aggregate formation. The Ric-3 that was not within aggregates co-localized with the ER marker (Fig. 4D). Many of the aggregated Ric-3 structures, however, did not co-localize with the ER marker while others did co-localize partially or co-localized completely (Fig. 4E). Consistent with this observation, we measured less (65%, $R = 0.47 \pm 0.05$, n=10 cells, supplemental Fig. 3F) of the CFP-Ric-3 overlap with the ER marker as compared to 86% overlap with low-levels of Ric-3. Again, there was no significant overlap of CFP-Ric-3 with the Golgi marker (1%, $R = 0.07 \pm 0.01$, n=10 cells, Fig. 4F and supplemental Fig. 3F). The results suggest that the aggregation initially occurs in the ER and later departs.

Effects of Ric-3 levels on α7 subunit and BgtR localization

We performed additional experiments to examine whether Ric-3 altered the subcellular distribution of α7 subunits or vice-versa. Cells were transfected with α7 subunit plasmid and no, low (0.01 μg) or high (5 μg) levels of Ric-3 plasmid and sorted using flow cytometry as in Fig. 2. The distribution of α7 subunits in the absence of Ric-3 was examined using anti-α7 Ab staining (Fig. 5A) and found to co-localized with the ER marker as has been previously observed (Cooper and Millar, 1997). The distribution of α7 co-expressed with low levels of Ric-3 was assayed using CFP-Ric-3 and is displayed in Fig. 5C and the inset. There was strong overlap between Ric-3, α7, and the ER marker consistent with ER localization when Ric-3 increases BgtR surface delivery (Fig. 1A). As in Fig. 2, we did not observe any significant co-localization of Ric-3 with the Golgi marker (data not shown) suggesting that Ric-3 again does not traffic with BgtRs out of the ER.

We used Fl-Bgt staining to assay the more mature, Bgt-binding pool of intracellular receptors. Surface BgtRs were excluded by binding surface BgtRs on intact cells with unlabeled Bgt prior to permeabilizing the cells. Bgt binding sites form on α7 subunits as they assemble into functional BgtRs in the ER (Rakhilin et al., 1999; Sweileh et al., 2000; Drisdel et al., 2004). Thus, Fl-Bgt should stain the pool of BgtRs assembling in the ER and a second pool of BgtRs that are released from the ER and trafficked to the cell surface. As expected, we did not detect Fl-Bgt staining in cells expressing α7 subunits without Ric-3 (Fig. 5B), conditions in which few to no BgtRs are assembled (Fig. 1A). At low levels of Ric-3, some of the intracellular Fl-Bgt staining coincided with the ER marker (Fig. 5D) just like the staining with anti-α7 Ab (Fig. 5C). These Fl-Bgt stained receptors were diffuse and of relatively weak intensity, consistent with a pool of intracellular BgtRs that are still assembling in the ER. In addition, Fl-Bgt stained

punctate structures throughout the cytoplasm (Fig. 5D and G). The size and shape of the punctate structures (diameter between 0.3 and 0.7 mm, n=20) were consistent with transport vesicles, in which the BgtRs had a higher fluorescence intensity (2.9 ± 0.3 fold, n=7 cells, 32 puncta) than the Fl-Bgt in the ER and, thus, 3-fold higher density (Fig 5D and inset). There was little co-localization between the punctate Fl-Bgt-stained structures and CFP-Ric-3, the ER (Fig. 5D) or Golgi markers (data not shown), consistent with these BgtR-containing structures being transport vesicles released from the ER and/or Golgi with BgtRs at a higher density.

To further test whether the Bgt-stained puncta had features expected of transport vesicles, we analysed whether the Bgt-stained puncta correlated with the surface delivery of BgtRs as a function of varying Ric-3 levels. In Fig. 5G we plotted the number of sorted cells with four or more Bgt-stained puncta at the different levels of Ric-3. Significant numbers of cells with Bgt-stained puncta were only observed in cells sorted for surface Fl-Bgt staining (Fl-Bgt+) at the different Ric-3 levels. Puncta were not observed in the absence of Ric-3 expression or for cells with no significant surface Bgt staining and positive for CFP-Ric-3 fluorescence. We previously reported the presence of Bgt-stained puncta in cells with α7/5HT3 BgtRs (Drisdel et al., 2004). Examples of these α7/5HT3 BgtR puncta are also displayed in supplemental Figs. 4A and B. In contrast to α7 BgtRs, α7/5HT3 BgtRs form and traffic to the cell surface very efficiently in the absence of Ric-3. Additionally, the surface and intracellular levels of α7/5HT3 BgtRs are much higher than that obtained with α7 BgtRs and low levels of Ric-3 do not affect the surface expression of α7/5HT3 BgtRs (Fig. 1B). We performed cell sorting and immunostaining experiments in which α7/5HT3 was transfected with or without low levels of CFP-Ric-3 (supplemental Figs. 4A and B). We found that in the absence or presence of low levels of CFP-Ric-3 virtually every cell contained Bgt-stained puncta. These findings are different from that with α7 BgtRs where no puncta were observed in the absence of Ric-3 and at best only ~40% of the cells had Bgt-stained puncta (Fig. 5G). Thus, for both α7 and α7/5HT3 BgtRs, the number of cells positive for Bgt-stained puncta correlates well with the levels of surface BgtR expression, another indication that the puncta are transport vesicles. Altogether the data are consistent with Ric-3, at low levels, facilitating the formation of BgtRs in the ER. Ric-3 may also help mediate the entry and increased density of BgtRs at ER release sites, where their exit in transport vesicles occurs. However, Ric-3 does not appear to enter the vesicles with the BgtRs as they traffic to the cell surface.

We also examined how high levels of Ric-3 altered BgtR localization (Fig. 5E and F). A significant change observed with high Ric-3 levels was the loss of surface delivery of BgtRs (Figs. 1 and 2) and loss of the BgtR-containing small puncta observed with low Ric-3 levels (Fig. 5G). Many of the aggregated structures observed with high levels of Ric-3 were stained with anti-α7 Abs (Fig. 5E and inset) and with Fl-Bgt (Fig. 5F). We observed a similar change in the distribution of α7/5HT3 BgtRs in the presence of high levels of Ric-3 (supplemental Fig. 4C). In addition to the aggregates, we observed significant levels of anti-α7 Ab and Fl-Bgt staining diffusely co-localized with Ric-3 in the ER of these cells. We estimated the total cellular Fl-Bgt and that portion that co-localized with the aggregates 36 hours after transfection when surface ^{125}I-Bgt binding peaked. At this time, we found that 67% of BgtRs were in the aggregates and 33% of BgtRs were not aggregated and were diffusely distributed with Ric-3 in the ER. One possibility is that BgtRs associate with aggregated Ric-3 and this association retains BgtRs in the ER reducing the amount of BgtRs available for surface transport. Because at high Ric-3 levels so few of the intracellular BgtRs arrive on the cell surface (~10% of α7 BgtRs; Fig. 1) despite a significant pool of diffuse BgtRs, another possibility is that the diffuse Ric-3, not the aggregated Ric-3, retains BgtRs in the ER. Many of the aggregated structures that contain Ric-3 and α7 subunits do not co-localize with the ER marker (Fig. 4D and E) consistent with the structures moving out of the ER. These data suggest that Ric-3 at high levels prevents BgtRs assembled in the ER from entering transport vesicles and retains BgtRs in the

ER. Retained BgtRs complexed with Ric-3 subsequently aggregate and the aggregates somehow depart the ER.

Native Ric-3 in PC12 cells

To further investigate the relationship between Ric-3 levels and BgtR expression, we assayed Ric-3 in cells with endogenous Ric-3 and BgtRs. We first examined the rat pheochromocytoma cell line, PC12 (N21 variant (Blumenthal et al., 1997; Rangwala et al., 1997)), to assay the levels of endogenous Ric-3 and compare its distribution relative to that of endogenous α7 subunits. The levels of α7 BgtRs on the surface of PC12 cells (~0.15 pmol/mg, data not shown) were somewhat less than the peak levels we observed in HEK cells co-expressed with α7 subunit and Ric-3 plasmids (Fig. 1A). Ric-3 mRNA is found in PC12 cells (Williams et al., 2005), but we were unable to detect Ric-3 by immunoblot analysis with similar levels of total cellular protein (data not shown). This finding indicates that the levels of Ric-3 in PC12 cells are less than what we obtained with heterologous expression in the range of 0.05 to 0.01 μg Ric-3 plasmid (Fig. 1C). To confirm the presence of Ric-3 mRNA in our PC12 cells, we performed RT-PCR and observed a band at the expected size for rat Ric-3 (data not shown). We observed immunostaining of the PC12 cells with Ric-3-specific Abs (Fig. 6A) not observed with a pre-immune serum control (data not shown). The pattern and levels of staining were similar to that observed in 20% of HEK cells with low levels of Ric-3 (Fig. 2E, H) consistent with the presence of the Ric-3 protein in the PC12 cells. As assayed by immunofluorescence, Ric-3 was present in virtually all PC12 cells (Fig. 6A), co-localized with α7 subunits, and varied in expression levels over a 2-fold range (Fig. 6B). The ability of the Ric-3 Ab to stain the PC12 cells but not the corresponding immunoblots suggested that the Ric-3 Ab affinity is dependent on the epitope conformation.

Based on several observations, the levels and distribution of Ric-3 in PC12 cells were similar to that seen in HEK cells expressing low levels of Ric-3. First, increasing levels of Ric-3 correlated with increased levels of surface and internal BgtRs as assayed by Fl-Bgt staining (Fig. 6B) similar to what we observed with low levels of Ric-3, but not for high levels of Ric-3, in the HEK cells (Fig. 1A). As observed in the HEK cells, none of the Ric-3 staining in the PC12 cells co-localized with the surface Fl-Bgt staining (Fig. 6C). Second, Ric-3 had a diffuse, perinuclear distribution in the PC12 cells that was highly co-localized with ER markers as well as with α7 subunits (Fig. 6D), consistent with an ER localization. None of the Ric-3 aggregation observed with high levels of Ric-3 in HEK cells was observed in the PC12 cells. Third, with Fl-Bgt intracellular staining we also observed two pools of intracellular BgtRs (Fig. 6E) similar to that observed in HEK cells. The first pool was diffuse, of weaker intensity and highly co-localized with Ric-3 staining. The second pool were in puncta with the features of transport vesicles in that the Fl-Bgt staining did not co-localize with Ric-3 or ER staining and had a 3-fold higher fluorescence intensity than the first pool (3.2 ± 0.3 fold, n=10 cells, 61 puncta; Fig 6E).

Ric-3 and α7 subunits in neurons

We also examined native Ric-3 in primary cultures of rat hippocampal neurons and compared its distribution to that of α7 subunits. Previous studies found that 60 – 100% of the GABAergic interneurons in neuronal cultures contain α7 subunits (Liu et al., 2001; Kawai et al., 2002), which are 7 to 15% of the total neurons. These finding are consistent with results from slices and sections taken from adult hippocampi where it was observed that ^{125}I-Bgt binding sites and functional BgtRs are found predominantly on GABAergic interneurons (Jones and Yakel, 1997; Frazier et al., 1998; Albuquerque et al., 2009). We observed a similar distribution of α7 subunits and GABAergic neurons in our cultures using staining for glutamic acid decarboxylase (GAD; see Table 1). As shown in Fig. 7A and Table 1, there is a strong correspondence between neurons that stain for Fl-Bgt, Ric-3 and anti-GAD. Furthermore, like

α7 subunits (Kawai et al., 2002; Xu et al., 2006), Ric-3 is restricted to somata and dendrites, as shown by its co-localization with microtubule-associated protein 2 (MAP2), and is not found in axons as shown by a lack of co-localization with neurofilament heavy chain (NFH) in axons (Fig. 7B). As in PC12 cells, Ric-3 closely co-localized with the ER marker. In somata (Fig. 7C), the staining was similar to the perinuclear distribution seen in PC12 cells and HEK cells with low levels of Ric-3. There was also a high degree of co-localization between Ric-3 and α7 (Fig. 7D) in the ER as in PC12 and HEK cells. Much of the Fl-Bgt in somata was diffuse and co-localized with Ric-3 (Fig. 7E) in the ER. Fl-Bgt puncta with 3-fold higher fluorescence intensity (3.3 ± 0.3 fold, n=6 cells, 27 puncta; Fig. 7E inset) were also observed. There may have been some co-localization between the Fl-Bgt puncta and Ric-3 in the perinuclear region but we believe that this was caused by the close proximity of the Fl-Bgt puncta, which appear to be transport vesicles. Fl-Bgt puncta that we observed further from the ER in somata clearly showed no co-localization with Ric-3 (Fig. 7E, inset).

As with PC12 cells, the expression levels of Ric-3 in the somata of the neurons varied over a 2-fold range. Levels of Ric-3 in neurons were significantly higher than in PC12 cells yet there were no signs of Ric-3 aggregation as was observed with higher levels in HEK cells. Compared to the levels of Ric-3 in PC12 cells (1.0 ± 0.06 fold, n=67 cells), Ric-3 levels in neurons were approximately 3-fold higher (2.8 ± 0.11 fold, n=94 cells; $p<0.001$). Because Ric-3 is restricted to the ER as in HEK and PC12 cells, we were initially surprised by the levels of Ric-3 in the dendrites. However, in dendrites Ric-3 co-localizes with the ER marker in the shafts (Fig. 7F) consistent with Ric-3 present in the ER sub-compartment that exists throughout dendrites (Bannai et al., 2004;Mironov and Symonchuk, 2006). α7 subunits are found throughout the dendrites and co-localized with Ric-3 (Fig. 7G) in the ER sub-compartment. To label intracellular receptors with Fl-Bgt, surface BgtRs were blocked with unlabeled Bgt. We found brightly stained Fl-Bgt puncta throughout the dendrites (Fig. 7H), which did not co-localize with Ric-3 or the ER marker. There was also weak and diffuse Fl-Bgt staining in the shafts that appeared to co-localize with Ric-3.

To better visualize Ric-3 in neurons, we transfected neurons with CFP-Ric-3 (Fig. 8). Most transfections of CFP-Ric-3 did not significantly increase total Ric-3 above normal levels, and CFP-Ric-3 showed a diffuse reticulated pattern in the somata similar to endogenous Ric-3 and co-localized in the ER (Fig 8A, left). When CFP-Ric-3 was transfected at higher levels, we occasionally observed aggregates indicating that we were over-expressing Ric-3 as observed in HEK at high levels (Fig. 8A, right). At the lower levels, CFP-Ric-3 was distributed in the somata and dendrites but not in axons (Fig. 8B) indicating that at these levels CFP-Ric-3 had the expected distribution. Furthermore, transfection of CFP-Ric-3 did not significantly interfere with the assembly and surface transport of native BgtRs as shown by strong surface Fl-Bgt staining of endogenous BgtRs in transfected neurons (Fig. 8C). As observed in PC12 and HEK cells, none of the Ric-3 colocalized with surface Fl-Bgt staining (Fig. 8C inset).

In the somata, CFP-Ric-3 co-localized with transfected α7-HA subunits in the ER labeled by DsRed-ER (Fig. 8D). We only analyzed transfected GABAergic interneurons by anti-GAD immunostaining (not shown). In dendrites, CFP-Ric-3, α7-HA subunits and the ER sub-compartment labeled with DsRed-ER were better resolved than endogenous α7 subunits (Fig 8E). We determined the degree of colocalization and the coefficients of colocalization, R, and found that α7 subunits and Ric-3 in dendrites were highly co-localized with the ER sub-compartment as was observed with endogenous Ric-3. 83% of the ER marker pixels co-localized with α7 subunits (R = 0.74 ± 0.03, n=10 neurons) and 80% with CFP-Ric-3 (R = 0.67 ± 0.04, n=12 neurons) indicating strong co-localization. There was also strong co-localization between α7 and CFP-Ric-3 (R = 0.71 ± 0.04, n=13 neurons). When we stained for intracellular BgtRs, we observed two distributions of Fl-Bgt staining in the somata similar to what we observed in HEK and PC12 cells: a diffuse pool that co-localized with CFP-Ric-3 and bright

Fl-Bgt puncta (Fig. 8F). In the dendrites, we clearly resolved two different types of staining that contained α7 subunits. The first type contained α7-HA subunits, CFP-Ric-3, DsRed-ER and either no staining or light staining with Fl-Bgt (Figs. 8E,G). This type of staining, while generally diffuse and reticulated as in the somata, also consisted of smaller puncta (see Fig. 8H). The second type of α7 subunit structures in dendrites, while fewer in number than the first type, contained Fl-Bgt at higher intensity but no Ric-3 or DsRed-ER (Fig. 8G). These structures were similar in appearance to the Fl-Bgt transport vesicles found in the somata (Fig. 8F). We often observed these structures in close apposition to ER sub-compartment membranes that contained Ric-3 (Fig. 8I) and α7 subunits (data not shown), which suggested that the BgtR containing puncta budded from the ER sub-compartment membranes.

Why do Ric-3 and α7 subunits co-localize to the ER sub-compartment of dendrites? One possibility is that Ric-3 and/or α7 subunit mRNA are transported to sites in dendrites where they are translated via local protein synthesis (Martin and Zukin, 2006) and synthesized at the ER sub-compartment. To test for this, we transfected cultured neurons with different combinations of the plasmids for CFP-Ric-3, HA-tagged α7 subunits (α7-HA) and the ER marker, DsRed-ER, which co-localizes well with the dendritic ER sub-compartment (Bannai et al., 2004). Previous studies of transfected α7 subunits (Xu et al., 2006) and DsRed-ER (Bannai et al., 2004) found that their basic properties in terms of their expected distribution in the neurons were not altered. Virtually all of the transfected CFP-Ric-3, α7-HA subunits and DsRed-ER appeared first in the somata before we observed their staining in the dendrites (data not shown). This finding does not rule out the possibility that some local dendritic synthesis is occurring but does indicate that the bulk of these proteins is synthesized in the somatic ER and then transported out to the dendrites.

Another possible explanation for why Ric-3 and α7 subunits co-localize to the ER sub-compartment of dendrites is that ER sub-compartment is the compartment in which α7 subunits are trafficked along dendrites. The ER sub-compartment in dendrites has a dedicated transport system composed of small vesicles that traffic proteins synthesized in the somatic ER to the dendritic ER sub-compartment (Bannai et al., 2004; Mironov and Symonchuk, 2006). NMDA-type glutamate receptors (NMDARs) are trafficked via this pathway and bypass the Golgi in somata if associated with SAP97 (Jeyifous et al., 2009). Thus, Ric-3 could play a similar role as SAP97 and α7 subunits could be trafficked from the ER in the soma via the ER sub-compartment in dendrites.when associated with Ric-3. To test for this possibility, we performed additional experiments to determine whether α7 subunits, when complexed with Ric-3, are trafficked from the ER in the soma via the ER sub-compartment in dendrites. If Ric-3 is synthesized in the somatic ER and trafficked to dendrites via the ER sub-compartment, we would predict that Ric-3, which is highly co-localized with α7 subunits in dendrites, should be observed in rapidly moving puncta (0.2–0.3 μm/sec; see (Bannai et al., 2004)). We would also predict that the Ric-3 puncta should contain ER markers as previously observed (Bannai et al., 2004). To test these predictions, we performed time-lapse, live-imaging of neurons transfected with CFP-Ric-3 and the fluorescent ER marker DsRed-ER. A large number of the puncta containing both constructs was seen rapidly moving (0.22 ± 0.04 μm/sec, n=17 puncta) as shown in Fig. 8H. The high degree of colocalization between CFP-Ric-3, ER-DsRed and α7HA immunostaining strongly suggests that the moving CFP-Ric-3 and ER-DsRed puncta contain α7 subunits consistent with their transport via the ER sub-compartment. Another prediction is that changes in Ric-3 levels in the neurons should alter the trafficking of α7 subunits from the soma to dendrites. Ric-3 knockdown experiments would be difficult to interpret because at levels below detection by immunoblotting and immunofluorescence (Figs. 1 and 2) Ric-3 promotes BgtR assembly and release from the ER.

Discussion

In this study, we addressed how Ric-3 functions with respect to α7 subunits. The initial genetic screen and characterization of Ric-3 mutations in *C. elegans* indicated that Ric-3 had a role in nAChR assembly and/or trafficking (Halevi et al., 2002). The introduction of Ric-3 into cultured mammalian cells or *Xenopus* oocytes altered cell-surface and total expression of 5HT3 receptors and different nicotinic receptor subtypes but not other receptors such as AMPA receptors (Halevi et al., 2002; Halevi et al., 2003; Castillo et al., 2005). Ric-3 either promoted (Cheng et al., 2005; Cheng et al., 2007) or inhibited (Halevi et al., 2003) 5HT3A receptor surface levels. Results co-expressing Ric-3 with α4β2 nAChRs were also inconsistent. One study found that Ric-3 decreased whole-cell currents (Halevi et al., 2003) and another found that Ric-3 increased whole-cell epibatidine binding to nAChRs (Lansdell et al., 2005). The introduction of Ric-3 consistently enhanced surface expression of α7-containing BgtRs in a variety of expression systems (Halevi et al., 2002; Halevi et al., 2003; Ben-Ami et al., 2005; Castillo et al., 2005; Lansdell et al., 2005; Williams et al., 2005; Castillo et al., 2006; Wang et al., 2009), though the degree of the enhancement was variable. These discrepancies can be explained by our findings that Ric-3's function changes dependent on Ric-3 levels. In cases where the number of cell-surface receptors increased, our data indicate that Ric-3 levels were low enough that Ric-3 increased BgtR formation and ER release. In cases with decreased cell-surface expression, levels of Ric-3 high enough to cause receptor ER retention explain the results. In all studies, surface expression of α7-containing BgtRs was enhanced by Ric-3 because the number of surface BgtRs was not significant in the absence of Ric-3. Thus, even at the highest Ric-3 levels there was a net increase in the number of surface α7-containing BgtRs (Fig. 1A).

Differences were also reported in studies examining where Ric-3 resides in cells. Most studies found Ric-3 predominantly in the ER (Castillo et al., 2005; Cheng et al., 2005; Cheng et al., 2007; Wang et al., 2009), where it is synthesized. However, Ric-3 has also been reported to co-localize with nAChRs at the cell surface (Williams et al., 2005) and in the Golgi apparatus (Castillo et al., 2005; Cheng et al., 2007). When we transfected low levels of Ric-3 into HEK cells, Ric-3 co-localized with markers of the ER but did not co-localize with markers of the Golgi apparatus or at the cell surface. Similar results were obtained for endogenous Ric-3 in PC12 cells and cultured neurons. In these cells, native Ric-3 again was localized to the ER and not to the Golgi apparatus or cell-surface. In neurons, the localization in the ER extended from the soma into the dendrites where we observed that Ric-3 trafficked in transport vesicles. These vesicles appeared to be a part of the ER sub-compartment of dendrites (Spacek and Harris, 1997; Toresson and Grant, 2005) and did not localize to "Golgi outposts" or the cell surface. Although we only found Ric-3 in the ER, it is still possible that Ric-3 traffics out of the ER to other compartments in the secretory pathway, but such departures must be rapid under normal circumstances.

We initially thought that the ER retention of α7 and α7/5HT3 subunits observed at high Ric-3 levels in HEK cells was an artifact caused by over-expression. We based this conclusion on the correlation between ER retention and aggregation and the finding that aggregation was not observed for endogenous Ric-3 in PC12 cells and neurons. As discussed in more detail below, subsequent observations suggested that native Ric-3 in cultured neurons can act to retain α7 subunits in the ER and this retention occurs without aggregates forming. The lack of Ric-3 aggregates in the neurons indicates that it is the "non-aggregated" or "free" Ric-3 that mediates subunit ER retention. ER retention of the subunits appears to result from a change in the nature of the interaction between Ric-3 and the subunits transitioning from a transient, short-lived interaction at low levels of Ric-3 to a more stable, long-lived interaction at higher levels. This is suggested by the ability to co-immunoprecipitate Ric-3 and the subunits at the higher Ric-3 levels and the extremely low levels of Ric-3 that increased BgtR formation and trafficking to

the surface (Fig. 1). Because Ric-3 is apparently an ER resident protein, long-lived interactions with Ric-3 could act to prevent interactions with COPII complex proteins that mediate release of membrane proteins from the ER. Ric-3 aggregates would form as Ric-3-subunit complexes accumulate in the ER and may involve a loss of ER-associated degradation (ERAD). The large aggregated Ric-3 structures we observed outside the ER of HEK cells with or without the subunits have the appearance of autophagosomes that can form when ERAD is overwhelmed and somehow depart the ER (e.g. (Kruse et al., 2006)).

Ric-3 trafficked differently in neurons than in PC12 or HEK cells. In cultured neurons, Ric-3 along with α7 subunits moved rapidly in puncta with the features of transport vesicles previously found to be part of the ER sub-compartment in dendrites (Bannai et al., 2004). Ric-3-containing puncta were not observed in PC12 or HEK cells and Ric-3 was clearly absent from the α7 subunit-containing puncta stained by Fl-Bgt that appeared to be transporting mature BgtRs to the surface of PC12 and HEK cells. Bgt-stained puncta that lacked Ric-3 were also present in the somata and dendrites of neurons. Our finding that significantly higher levels of native Ric-3 in the somata of neurons than in PC12 cells together with the co-localization of Ric-3 and α7 subunits in moving puncta that are part of the ER sub-compartment of dendrites suggests that the events depicted in Fig. 9 are occurring in neurons. In the model, Ric-3 has two separate functions regulated by the levels of Ric-3 available to interact with α7 subunits. At low levels (Fig. 9A and C), Ric-3 acts only to mediate BgtR folding and assembly. This appears to be how Ric-3 functions in PC12 cells and also in neurons when BgtRs are released from the ER in the soma and traffic via the somatic Golgi to the cell membrane. At higher levels in neurons, Ric-3 retains α7 subunits in the ER in addition to mediating BgtR folding and assembly (Fig. 9B). When restricted to the ER, complexes of Ric-3 and α7 subunits together remain within the ER sub-compartment and are transported on moving puncta in dendrites (Fig. 9C, red arrow pathway). We recently determined that NMDA-type glutamate receptors (NMDARs) in hippocampal neurons are also trafficked through such an “ER-restricted” pathway in dendrites (Jeyifous et al., 2009). Transport of NMDARs through the ER sub-compartment requires the presence of SAP97, which associate specifically with NMDAR NR2B subunits and, like Ric-3, acts to retain its binding partner in the ER of HEK cells. Thus, Ric-3 may have a role similar to SAP97 in retaining its binding partner in the ER sub-compartment. In neurons, the “ER-restricted” pathway taken by NMDARs sorts NMDARs from AMPA-type glutamate receptors, which are trafficked through the conventional secretory pathway in the soma (Jeyifous et al., 2009). After departing the ER sub-compartment, NMDA receptors traffic through Golgi outpost near spines (Jeyifous et al., 2009). Similarly, we assume that BgtRs are released from the ER sub-compartment and traffic through Golgi outposts before inserting in the plasma membrane (Fig. 9C). Consistent with this idea are the BgtR-containing puncta we observed in close opposition to the ER sub-compartment membranes in the dendrites (Fig. 8I). These puncta may traffic via Golgi outposts to the dendritic surface after release from the ER sub-compartment membranes.

As shown previously (Kawai et al., 2002; Xu et al., 2006), BgtRs are found on the somata and dendrites of cultured hippocampal neurons and do not traffic to axons. However, there is much evidence that BgtRs do traffic to axons in vivo and, in particular, to axon terminals where their activation can regulate the presynaptic release of neurotransmitters (Gray et al., 1996; Fabian-Fine et al., 2001). In cultured hippocampal neurons, BgtR axonal transport may be prevented in part by the relatively high levels of Ric-3 that restrict α7 subunits to the dendritic ER sub-compartment. If true, mechanisms should exist to regulate Ric-3 levels in cells. Recent work indicates that levels of Ric-3 are tightly regulated by the ubiquitin proteosome system in *C. Elegans* (Shteingauz et al., 2009). Mechanisms may also exist that regulate Ric-3 interactions with α7 subunits, thereby determining when BgtR is released from the ER sub-compartment in dendrites. An example of other membrane proteins regulated this way is the ER-retention of the proteins that mediate cholesterol homeostasis. The release of HMG CoA reductase and

other proteins involved in cholesterol homeostasis from the ER is regulated by sterol levels (Espenshade and Hughes, 2007; Sun et al., 2007). Ric-3 and the proteins that regulate α7 subunit assembly and trafficking may have a similar role to the proteins SCAP and Insig-1 and −2 that regulate HMG CoA reductase and sterol regulatory element binding protein assembly and trafficking.

Supplementary Material

Refer to Web version on PubMed Central for supplementary material.

Acknowledgments

This work was supported by grants: BFU2008-02160 and CSD2008-00005 (The Spanish Ion Channel Initiative-Consolider Ingenio 2010) from the Ministry of Science and Innovation of Spain (MC), National Institutes of Health (NIH) NS043782, DA019695 and the Peter F. McManus Foundation (WNG). AVK was supported by NIH grant DA11643A awarded to R. E. Oswald and G. P. Hess (Cornell University). We thank Okunola Jeyifous for comments on the manuscript, members of the Green lab for discussion and comments on the work and Dr. Vytas Bindokas for help with the microscopy.

References

Albuquerque EX, Pereira EF, Alkondon M, Rogers SW. Mammalian nicotinic acetylcholine receptors: from structure to function. Physiol Rev 2009;89:73–120. [PubMed: 19126755]

Bannai H, Inoue T, Nakayama T, Hattori M, Mikoshiba K. Kinesin dependent, rapid, bi-directional transport of ER sub-compartment in dendrites of hippocampal neurons. J Cell Sci 2004;117:163–175. [PubMed: 14676272]

Ben-Ami HC, Yassin L, Farah H, Michaeli A, Eshel M, Treinin M. RIC-3 affects properties and quantity of nicotinic acetylcholine receptors via a mechanism that does not require the coiled-coil domains. J Biol Chem 2005;280:28053–28060. [PubMed: 15932871]

Betz H, Graham D, Rehm H. Identification of polypeptides associated with a putative neuronal nicotinic acetylcholine receptor. J Biol Chem 1982;257:11390–11394. [PubMed: 7118888]

Blumenthal EM, Conroy WG, Romano SJ, Kassner PD, Berg DK. Detection of functional nicotinic receptors blocked by alpha-bungarotoxin on PC12 cells and dependence of their expression on post-translational events. J Neurosci 1997;17:6094–6104. [PubMed: 9236221]

Castelan F, Castillo M, Mulet J, Sala S, Sala F, Dominguez Del Toro E, Criado M. Molecular characterization and localization of the RIC-3 protein, an effector of nicotinic acetylcholine receptor expression. J Neurochem 2008;105:617–627. [PubMed: 18179477]

Castillo M, Mulet J, Gutierrez LM, Ortiz JA, Castelan F, Gerber S, Sala S, Sala F, Criado M. Dual role of the RIC-3 protein in trafficking of serotonin and nicotinic acetylcholine receptors. J Biol Chem 2005;280:27062–27068. [PubMed: 15927954]

Castillo M, Mulet J, Gutierrez LM, Ortiz JA, Castelan F, Gerber S, Sala S, Sala F, Criado M. Role of the RIC-3 protein in trafficking of serotonin and nicotinic acetylcholine receptors. J Mol Neurosci 2006;30:153–156. [PubMed: 17192664]

Chen D, Patrick JW. The alpha-bungarotoxin-binding nicotinic acetylcholine receptor from rat brain contains only the alpha7 subunit. J Biol Chem 1997;272:24024–24029. [PubMed: 9295355]

Cheng A, McDonald NA, Connolly CN. Cell surface expression of 5-hydroxytryptamine type 3 receptors is promoted by RIC-3. J Biol Chem 2005;280:22502–22507. [PubMed: 15809299]

Cheng A, Bollan KA, Greenwood SM, Irving AJ, Connolly CN. Differential subcellular localization of RIC-3 isoforms and their role in determining 5-HT3 receptor composition. J Biol Chem 2007;282:26158–26166. [PubMed: 17609200]

Conti-Tronconi BM, Dunn SM, Barnard EA, Dolly JO, Lai FA, Ray N, Raftery MA. Brain and muscle nicotinic acetylcholine receptors are different but homologous proteins. Proc Natl Acad Sci U S A 1985;82:5208–5212. [PubMed: 3860855]

Cooper ST, Millar NS. Host cell-specific folding and assembly of the neuronal nicotinic acetylcholine receptor alpha7 subunit. J Neurochem 1997;68:2140–2151. [PubMed: 9109542]

Drisdel RC, Green WN. Neuronal alpha-bungarotoxin receptors are alpha7 subunit homomers. J Neurosci 2000;20:133–139. [PubMed: 10627589]

Drisdel RC, Manzana E, Green WN. The role of palmitoylation in functional expression of nicotinic alpha7 receptors. J Neurosci 2004;24:10502–10510. [PubMed: 15548665]

Eertmoed AL, Vallejo YF, Green WN. Transient expression of heteromeric ion channels. Methods Enzymol 1998;293:564–585. [PubMed: 9711629]

Eisele JL, Bertrand S, Galzi JL, Devillers-Thiery A, Changeux JP, Bertrand D. Chimaeric nicotinic-serotonergic receptor combines distinct ligand binding and channel specificities. Nature 1993;366:479–483. [PubMed: 8247158]

Espenshade PJ, Hughes AL. Regulation of sterol synthesis in eukaryotes. Annu Rev Genet 2007;41:401–427. [PubMed: 17666007]

Fabian-Fine R, Skehel P, Errington ML, Davies HA, Sher E, Stewart MG, Fine A. Ultrastructural distribution of the alpha7 nicotinic acetylcholine receptor subunit in rat hippocampus. J Neurosci 2001;21:7993–8003. [PubMed: 11588172]

Frazier CJ, Rollins YD, Breese CR, Leonard S, Freedman R, Dunwiddie TV. Acetylcholine activates an alpha-bungarotoxin-sensitive nicotinic current in rat hippocampal interneurons, but not pyramidal cells. J Neurosci 1998;18:1187–1195. [PubMed: 9454829]

Grando SA, Horton RM, Mauro TM, Kist DA, Lee TX, Dahl MV. Activation of keratinocyte nicotinic cholinergic receptors stimulates calcium influx and enhances cell differentiation. J Invest Dermatol 1996;107:412–418. [PubMed: 8751979]

Gray R, Rajan AS, Radcliffe KA, Yakehiro M, Dani JA. Hippocampal synaptic transmission enhanced by low concentrations of nicotine. Nature 1996;383:713–716. [PubMed: 8878480]

Halevi S, McKay J, Palfreyman M, Yassin L, Eshel M, Jorgensen E, Treinin M. The C. elegans ric-3 gene is required for maturation of nicotinic acetylcholine receptors. EMBO J 2002;21:1012–1020. [PubMed: 11867529]

Halevi S, Yassin L, Eshel M, Sala F, Sala S, Criado M, Treinin M. Conservation within the RIC-3 gene family. Effectors of mammalian nicotinic acetylcholine receptor expression. J Biol Chem 2003;278:34411–34417. [PubMed: 12821669]

Hamill OP, Marty A, Neher E, Sakmann B, Sigworth FJ. Improved patch-clamp techniques for high-resolution current recording from cells and cell-free membrane patches. Pflugers Arch 1981;391:85–100. [PubMed: 6270629]

Ho SN, Hunt HD, Horton RM, Pullen JK, Pease LR. Site-directed mutagenesis by overlap extension using the polymerase chain reaction. Gene 1989;77:51–59. [PubMed: 2744487]

Jeyifous O, Schubert M, Specht CG, Waites CL, Lin E, Fujisawa S, Marshall J, Aoki C, Montgomery JM, Garner CC, Green WN. SAP97 and CASK mediate sorting of N-Methyl-D-Aspartate Receptors through a novel secretory pathway. Nature Neuroscience. 2009

Jones S, Yakel JL. Functional nicotinic ACh receptors on interneurones in the rat hippocampus. J Physiol 1997;504(Pt 3):603–610. [PubMed: 9401968]

Karlin A, Akabas MH. Toward a structural basis for the function of nicotinic acetylcholine receptors and their cousins. Neuron 1995;15:1231–1244. [PubMed: 8845149]

Kawai H, Zago W, Berg DK. Nicotinic alpha 7 receptor clusters on hippocampal GABAergic neurons: regulation by synaptic activity and neurotrophins. J Neurosci 2002;22:7903–7912. [PubMed: 12223543]

Kemp G, Bentley L, McNamee MG, Morley BJ. Purification and characterization of the alpha-bungarotoxin binding protein from rat brain. Brain Res 1985;347:274–283. [PubMed: 4063809]

Kruse KB, Brodsky JL, McCracken AA. Autophagy: an ER protein quality control process. Autophagy 2006;2:135–137. [PubMed: 16874086]

Lansdell SJ, Gee VJ, Harkness PC, Doward AI, Baker ER, Gibb AJ, Millar NS. RIC-3 enhances functional expression of multiple nicotinic acetylcholine receptor subtypes in mammalian cells. Mol Pharmacol 2005;68:1431–1438. [PubMed: 16120769]

Li Q, Lau A, Morris TJ, Guo L, Fordyce CB, Stanley EF. A syntaxin 1, Galpha(o), and N-type calcium channel complex at a presynaptic nerve terminal: analysis by quantitative immunocolocalization. J Neurosci 2004;24:4070–4081. [PubMed: 15102922]

Liu Y, Ford B, Mann MA, Fischbach GD. Neuregulins increase alpha7 nicotinic acetylcholine receptors and enhance excitatory synaptic transmission in GABAergic interneurons of the hippocampus. J Neurosci 2001;21:5660–5669. [PubMed: 11466437]

Manders EM, Stap J, Brakenhoff GJ, van Driel R, Aten JA. Dynamics of three-dimensional replication patterns during the S-phase, analysed by double labelling of DNA and confocal microscopy. J Cell Sci 1992;103(Pt 3):857–862. [PubMed: 1478975]

Marks JD, Bindokas VP, Zhang XM. Maturation of vulnerability to excitotoxicity: intracellular mechanisms in cultured postnatal hippocampal neurons. Brain Res Dev Brain Res 2000;124:101–116.

Martin KC, Zukin RS. RNA trafficking and local protein synthesis in dendrites: an overview. J Neurosci 2006;26:7131–7134. [PubMed: 16822966]

Miller KG, Alfonso A, Nguyen M, Crowell JA, Johnson CD, Rand JB. A genetic selection for Caenorhabditis elegans synaptic transmission mutants. Proc Natl Acad Sci U S A 1996;93:12593–12598. [PubMed: 8901627]

Mironov SL, Symonchuk N. ER vesicles and mitochondria move and communicate at synapses. J Cell Sci 2006;119:4926–4934. [PubMed: 17105774]

Nguyen M, Alfonso A, Johnson CD, Rand JB. Caenorhabditis elegans mutants resistant to inhibitors of acetylcholinesterase. Genetics 1995;140:527–535. [PubMed: 7498734]

Rakhilin S, Drisdel RC, Sagher D, McGehee DS, Vallejo Y, Green WN. alpha-bungarotoxin receptors contain alpha7 subunits in two different disulfide-bonded conformations. J Cell Biol 1999;146:203–218. [PubMed: 10402471]

Rangwala F, Drisdel RC, Rakhilin S, Ko E, Atluri P, Harkins AB, Fox AP, Salman SS, Green WN. Neuronal alpha-bungarotoxin receptors differ structurally from other nicotinic acetylcholine receptors. J Neurosci 1997;17:8201–8212. [PubMed: 9334396]

Rasband, WS. ImageJ. Bethesda, Maryland, USA: U. S. National Institutes of Health; 1997–2009.

Sekhon HS, Jia Y, Raab R, Kuryatov A, Pankow JF, Whitsett JA, Lindstrom J, Spindel ER. Prenatal nicotine increases pulmonary alpha7 nicotinic receptor expression and alters fetal lung development in monkeys. J Clin Invest 1999;103:637–647. [PubMed: 10074480]

Shteingauz A, Cohen E, Biala Y, Treinin M. The BTB-MATH protein BATH-42 interacts with RIC-3 to regulate maturation of nicotinic acetylcholine receptors. J Cell Sci 2009;122:807–812. [PubMed: 19223395]

Spacek J, Harris KM. Three-dimensional organization of smooth endoplasmic reticulum in hippocampal CA1 dendrites and dendritic spines of the immature and mature rat. J Neurosci 1997;17:190–203. [PubMed: 8987748]

Sun LP, Seemann J, Goldstein JL, Brown MS. Sterol-regulated transport of SREBPs from endoplasmic reticulum to Golgi: Insig renders sorting signal in Scap inaccessible to COPII proteins. Proc Natl Acad Sci U S A 2007;104:6519–6526. [PubMed: 17428919]

Sweileh W, Wenberg K, Xu J, Forsayeth J, Hardy S, Loring RH. Multistep expression and assembly of neuronal nicotinic receptors is both host-cell- and receptor-subtype-dependent. Brain Res Mol Brain Res 2000;75:293–302. [PubMed: 10686351]

Toresson H, Grant SG. Dynamic distribution of endoplasmic reticulum in hippocampal neuron dendritic spines. Eur J Neurosci 2005;22:1793–1798. [PubMed: 16197520]

Udgaonkar JB, Hess GP. Chemical kinetic measurements of a mammalian acetylcholine receptor by a fast-reaction technique. Proc Natl Acad Sci U S A 1987;84:8758–8762. [PubMed: 2447583]

Wang H, Yu M, Ochani M, Amella CA, Tanovic M, Susarla S, Li JH, Yang H, Ulloa L, Al-Abed Y, Czura CJ, Tracey KJ. Nicotinic acetylcholine receptor alpha7 subunit is an essential regulator of inflammation. Nature 2003;421:384–388. [PubMed: 12508119]

Wang Y, Yao Y, Tang XQ, Wang ZZ. Mouse RIC-3, an endoplasmic reticulum chaperone, promotes assembly of the alpha7 acetylcholine receptor through a cytoplasmic coiled-coil domain. J Neurosci 2009;29:12625–12635. [PubMed: 19812337]

Whiting P, Lindstrom J. Purification and characterization of a nicotinic acetylcholine receptor from rat brain. Proc Natl Acad Sci U S A 1987;84:595–599. [PubMed: 3467376]

Williams ME, Burton B, Urrutia A, Shcherbatko A, Chavez-Noriega LE, Cohen CJ, Aiyar J. Ric-3 promotes functional expression of the nicotinic acetylcholine receptor alpha7 subunit in mammalian cells. J Biol Chem 2005;280:1257–1263. [PubMed: 15504725]

Xu J, Zhu Y, Heinemann SF. Identification of sequence motifs that target neuronal nicotinic receptors to dendrites and axons. J Neurosci 2006;26:9780–9793. [PubMed: 16988049]

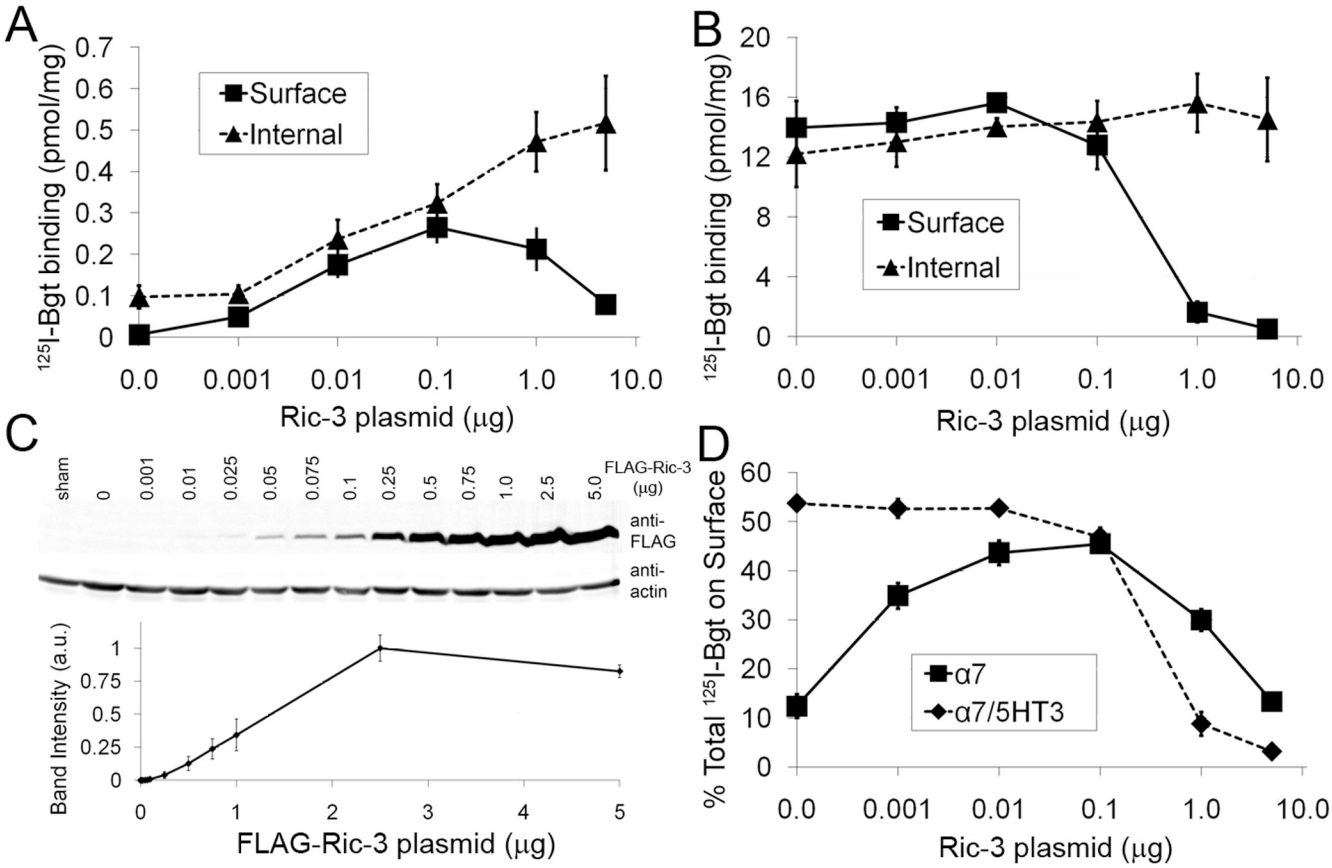

Figure 1. The dependence of BgtR expression on Ric-3 levels

Surface and internal BgtR expression were assayed by ^{125}I-Bgt binding, which is displayed as pmol ^{125}I-Bgt per mg total cellular protein. ^{125}I-Bgt binding assays were performed using transiently transfected HEK cells with set amounts of α7 **(A)** or α7/5HT3A **(B)** subunits (5 μg plasmid) and varying amounts of Ric-3 plasmid as shown. **(C)** Immunoblots and quantification of FLAG-tagged Ric-3 protein levels at the indicated plasmid levels. **(D)** Displayed is the cell-surface to total ratio of ^{125}I-Bgt binding sites.

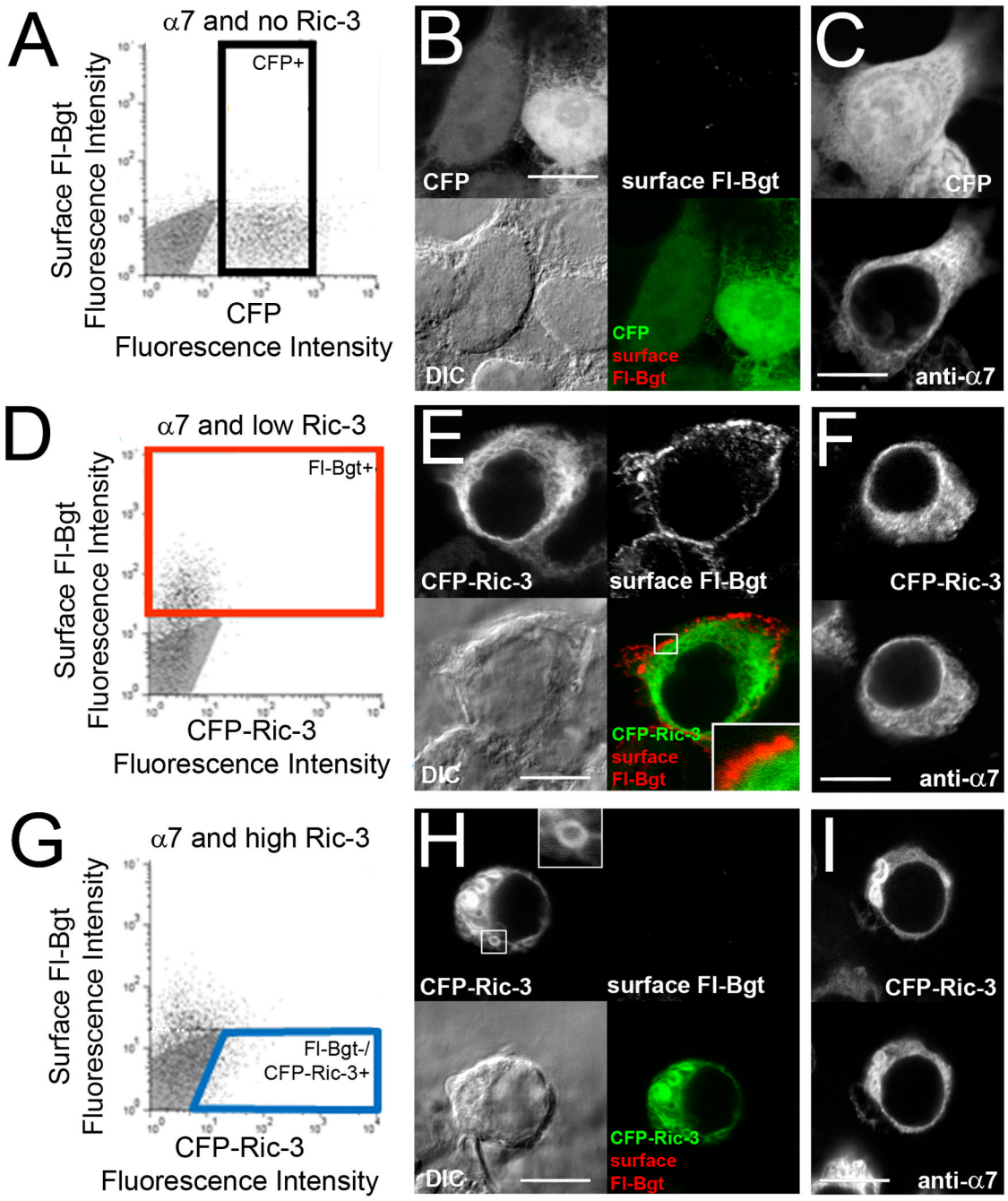

Figure 2. The cellular distribution of BgtRs and Ric-3 at different Ric-3 levels

We used flow cytometry to isolate representative cells for immunofluorescence analysis. To identify cells expressing BgtRs and different levels of Ric-3, cells were sorted using surface Fl-Bgt fluorescence and CFP or CFP-Ric-3 fluorescence. We performed three separate transfections each with a set amount of α7 subunit plasmid and varying amounts of Ric-3 plasmid: **(A–C)** No Ric-3, where α7 subunit expression was monitored using co-transfection with a CFP plasmid (pECFP); **(D–F)** low Ric-3 (0.01 μg CFP-Ric-3 plasmid) or **(G–I)** high Ric-3 (0.1 μg CFP-Ric3 and 4.9 μg Ric-3 plasmids). In panels **A, D**, and **G**, surface BgtRs were labeled with Fl-Bgt and points on the graphs represent single-cell fluorescence values for CFP or CFP-Ric-3 (x-axis) and Fl-Bgt (y-axis). The grey areas represent the level of non-

specific Fl-Bgt staining and/or autofluorescence of sham transfected cells. The horizontal line in each panel marks the maximum level of non-specific Fl-Bgt staining of sham transfected cells. In **A**, cells expressing α7 subunits without Ric-3 were selected (boxed group, CFP+) only using CFP fluorescence because there was no significant Fl-Bgt fluorescence. In **D**, cells expressing significant amounts of surface BgtRs were selected (boxed group, Fl-Bgt+) only using Fl-Bgt because there was no significant CFP-Ric-3 fluorescence at the low Ric-3 levels. In **G**, cells expressing high Ric-3 levels without surface BgtRs were selected (boxed group, Fl-Bgt-/CFP-Ric-3+) using CFP-Ric-3 fluorescence and an absence of any significant Fl-Bgt fluorescence. In the other panels are displayed examples of sorted cells typical of the three different transfections. In **B, E** and **H** are the following four images of the same cell set: 1) cell surface BgtRs labeled with Fl-Bgt are displayed (upper right), 2) CFP or CFP-Ric-3 (upper left), DIC (lower left) and 4) merged image of 1 and 2 (lower right). The boxed area in **E**, lower right is magnified in the inset to show the lack of overlap between surface BgtRs and CFP-Ric-3. The boxed area in **H**, upper left is magnified in the inset to show the features of the Ric-3 aggregates. In **C, F**, and **I**, are the following two images of the same cell set: 1) CFP or CFP-Ric-3 (upper) and 2) all α7 subunits labeled with anti-α7 Abs. Scale bars, 10 μm.

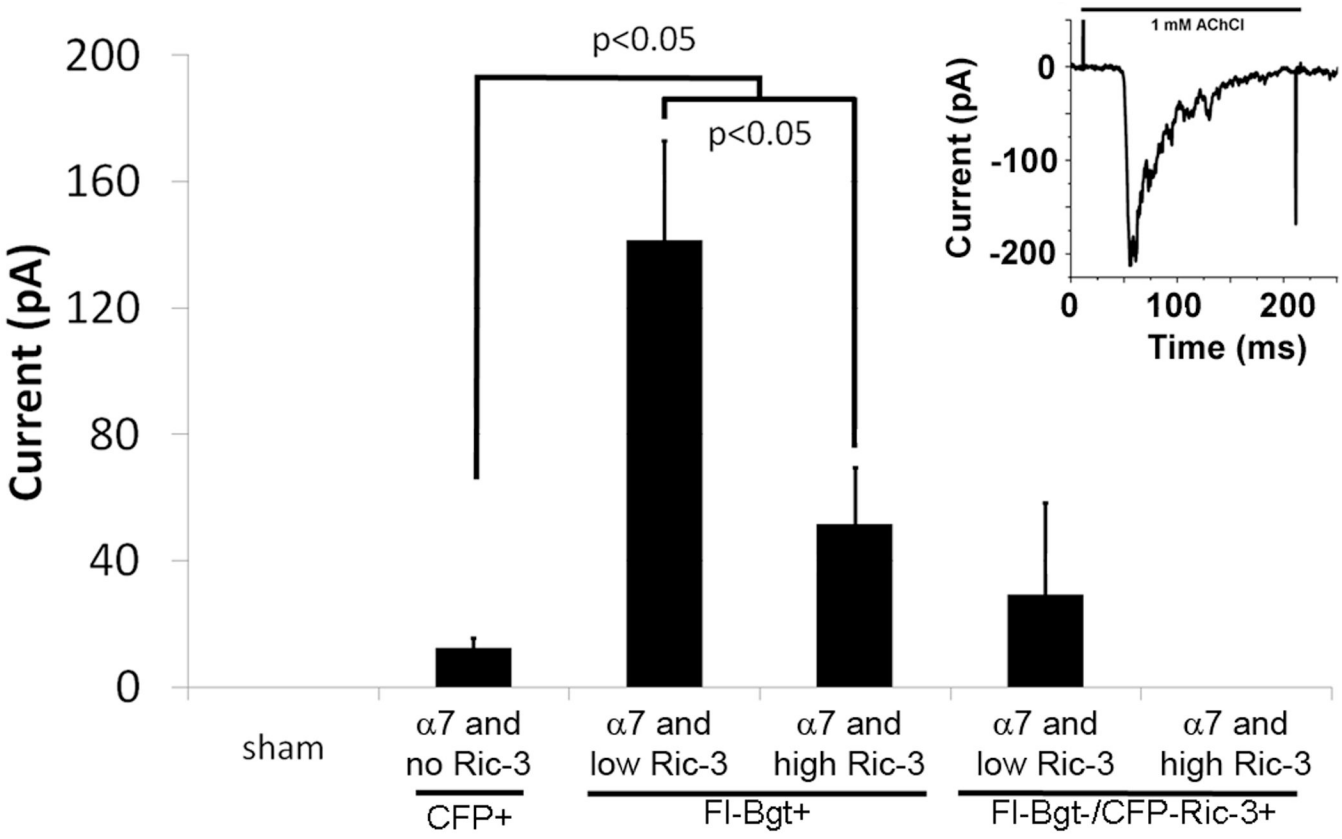

Figure 3. Effect of Ric-3 mediated on ACh-evoked currents of BgtRs

We performed whole-cell patch clamp recordings on cells expressing α7 subunits and no Ric-3, low levels of Ric-3 and high levels of Ric-3 as in Fig. 2. Cells were sorted as in Fig. 2 for CFP fluorescence (CFP+), Fl-Bgt fluorescence (Fl-Bgt+) or for Ric-3 fluorescence and no Fl-Bgt fluorescence (Fl-Bgt-/CFP-Ric-3+). Displayed are mean current amplitudes in response to the application of saturating ACh (1 mM) for cells sorted by CFP fluorescence expressing α7 and no Ric-3 (n=16), cells sorted by Fl-Bgt fluorescence with low levels of Ric-3 (n=28), or high levels of Ric-3 (n=15) when compared to sham transfected cells (n=5). A current response recorded after application of saturating ACh (1 mM; denoted by line above the current trace) is displayed in the **inset**. The spikes corresponding to the beginning and end of ACh application were artifacts caused by opening and closing of the solenoid valve. Cells sorted by having a significant amount of Fl-Bgt fluorescence had significantly higher current amplitudes than α7 expressing cells with no Ric-3 ($p<0.05$). Cells transfected with high amounts of Ric-3 had significantly smaller current amplitudes than those cells transfected with low amounts of Ric-3 ($p<0.05$). There were no ACh-evoked currents from sham transfected cells or cells sorted with no significant Fl-Bgt fluorescence and high levels of Ric-3 (n=6) and only one cell sorted with no significant Fl-Bgt fluorescence and low levels of Ric-3 exhibited a current response (n=5).

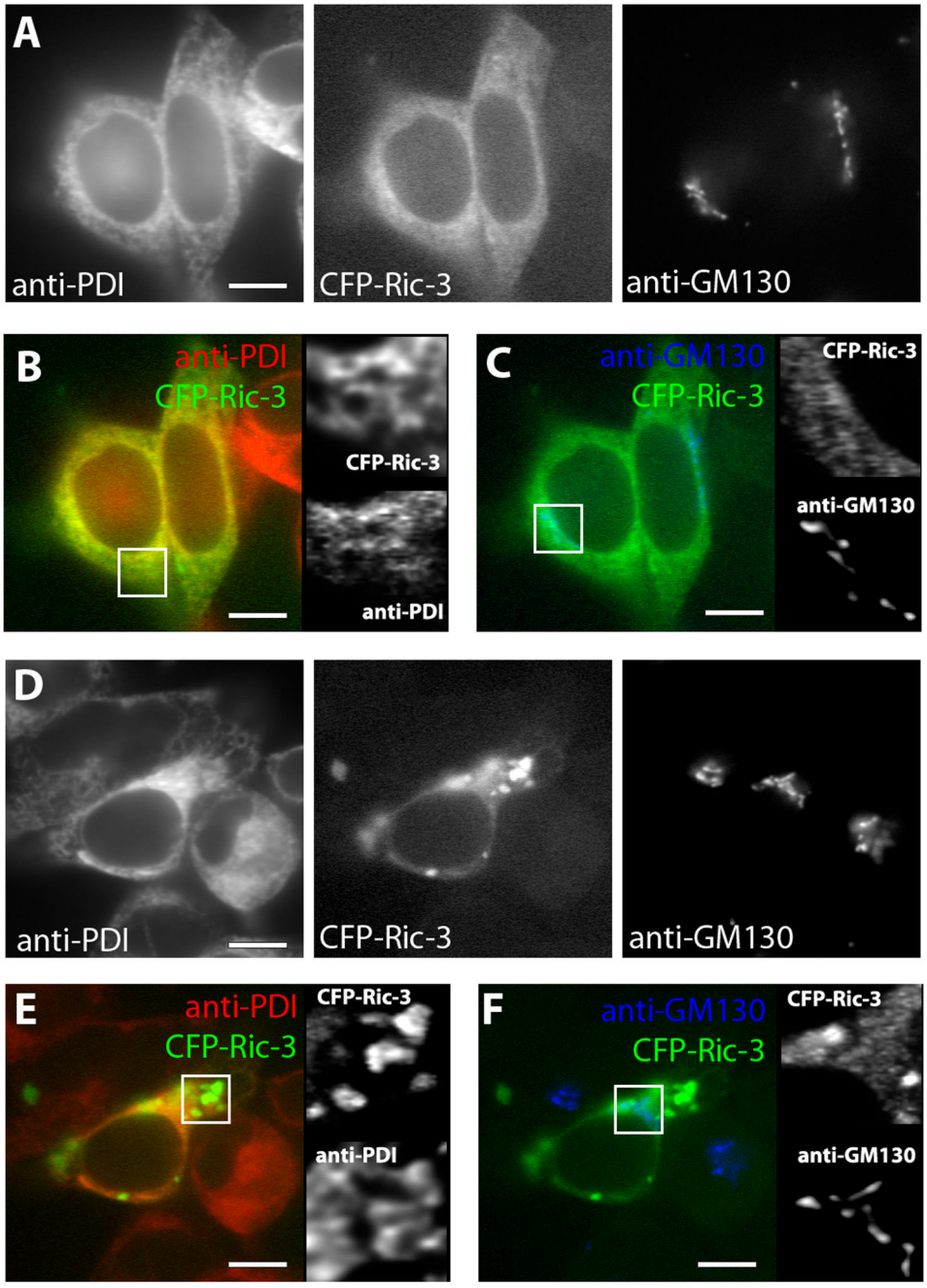

Figure 4. Cellular localization of Ric-3 in the absence of α7 subunits

Cells expressing low or high levels of Ric-3 without α7 subunits were sorted as in Fig. 2. **(A)** Sorted cells with low levels of Ric-3 were stained with Abs specific for an ER marker (anti-PDI) and a Golgi marker (anti-GM-130). **(B and C)** Merged images of the cells from **A** showing the degree of co-localization between CFP-Ric-3 and the ER marker **(B)** or Golgi marker **(C)**. To the right are enlarged views of the boxed regions in the panels. **(D)** Sorted cells with high levels of Ric-3 were stained with Abs specific for an ER marker (anti-PDI) and a Golgi marker (anti-GM-130). **(E and F)** Merged images of the cells from **E** showing the degree of co-localization between CFP-Ric-3 and the ER marker **(E)** or Golgi marker **(F)**. To the right are enlarged views of the boxed regions in the panels. Scale bars, 10 μm.

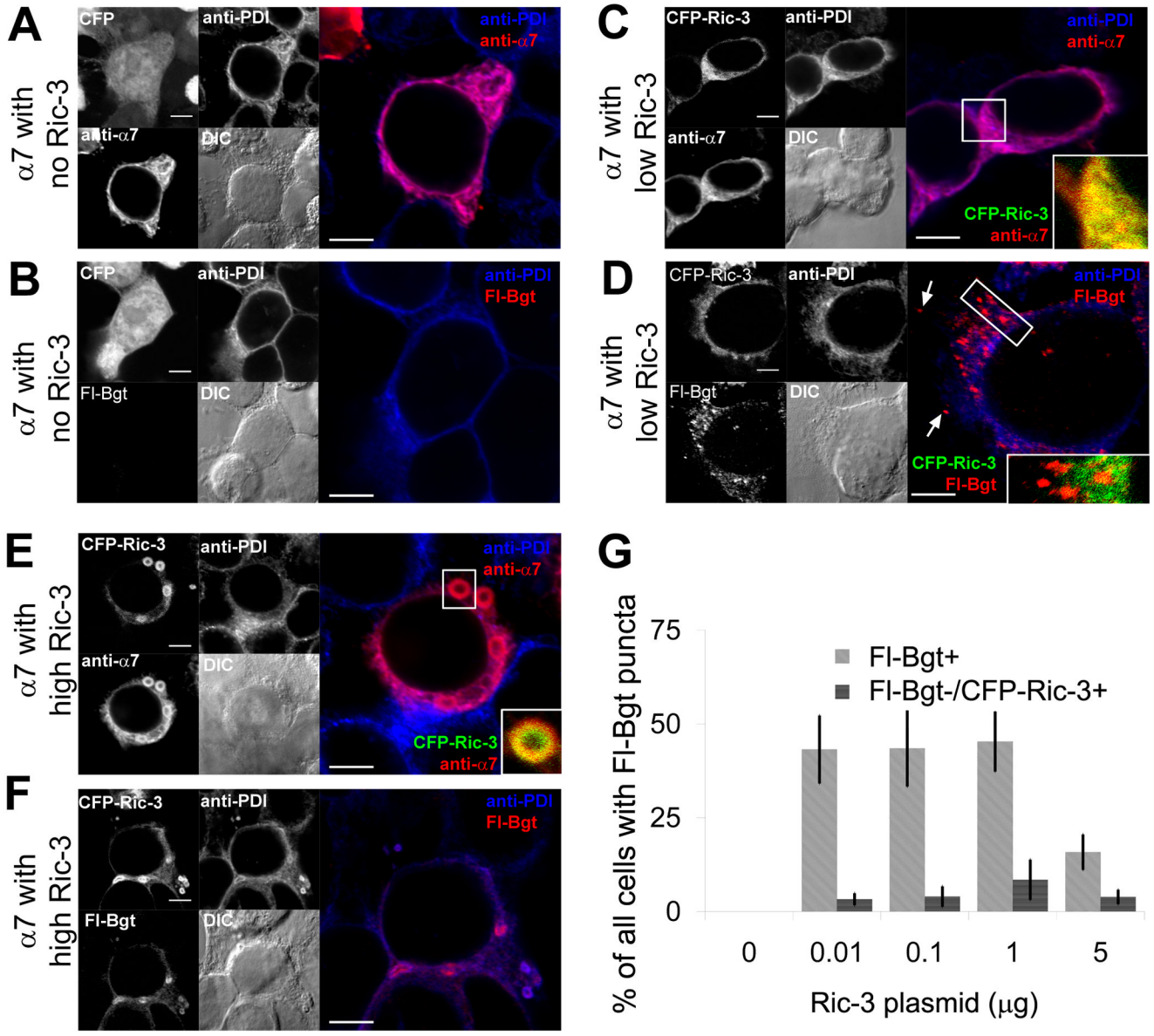

Figure 5. Cellular localization of Ric-3 and α7 subunits

As in Fig. 2, cells expressing α7 subunits and no Ric-3 (**A** and **B**), low levels of Ric-3 (**C** and **D**) and high levels of Ric-3 (**E** and **F**) were sorted. Images of typical cells are displayed for the different levels of Ric-3. The left half of each panel is divided into four sections: 1) the CFP fluor used for sorting (upper left), 2) the ER marker (anti-PDI Ab; upper right), 3) the α7 subunit-specific marker (anti-α7 Ab or Fl-Bgt; lower left) and 4) the DIC image (lower right). On the right half are merged images of 2 and 3. **(A)** Cells were stained for α7 subunits and the ER. **(B)** Cells were stained for intracellular BgtRs and the ER. **(C)** Cells were stained for α7 subunits and the ER. A higher magnification of the boxed region in the merged image is displayed in the inset and is a merged image of the CFP-Ric-3 and anti-α7 Ab fluorescence. **(D)** Cells were stained for intracellular BgtRs and the ER. With low Ric-3 levels, we observed bright puncta stained with Fl-Bgt. A higher magnification of the puncta in the boxed region in the merged image is displayed in the inset and is a merged image of the CFP-Ric-3 and Fl-Bgt fluorescence. **(E)** Cells were stained for α7 subunits and the ER marker. With high Ric-3 levels,

we observed Ric-3 aggregates stained with anti-α7 and Fl-Bgt. A higher magnification of the boxed region in the merged image is displayed in the inset and is a merged image of the CFP-Ric-3 and anti-α7 Ab fluorescence. **(F)** Cells were stained for intracellular BgtRs and the ER. **(G)** Cells were sorted and stained as in **D** or **F** and we determined the percent of sorted cells that had 4 or more Fl-Bgt-stained puncta. On the Y axis we plotted the percent of total cells with 4 or more Fl-Bgt-stained puncta at the indicated levels of Ric-3 for cells sorted for Fl-Bgt fluorescence (Fl-Bgt+) or for cells lacking Fl-Bgt fluorescence but positive for CFP-Ric-3 fluorescence (Fl-Bgt-/CFP-Ric-3+). Scale bars, 5 μm.

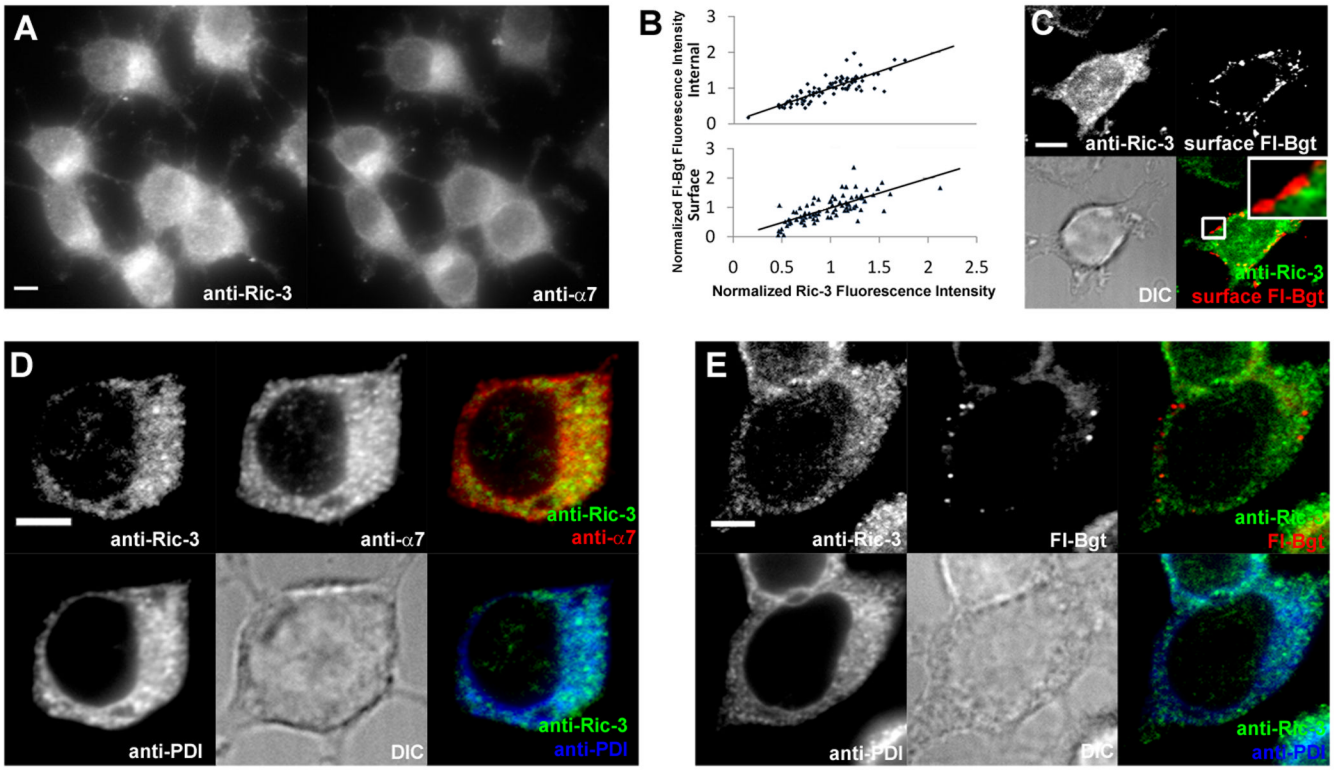

Figure 6. Native Ric-3 in PC12 cells

(A) PC12 cells were immunostained with Abs specific for Ric-3 (left) and anti-α7 subunits (right). **(B)** Relation between intracellular and surface BgtR levels as determined by Fl-Bgt labeling (Y-axis) and Ric-3 levels as determined by staining with Ric-3-specific Abs (X-axis). **(C)** PC12 cells were labeled with Fl-Bgt on the cell surface, permeabilized, then stained using the anti-Ric-3 Ab. **(D)** Staining with anti-Ric-3, anti-α7, and anti-PDI (ER marker) Abs. **(E)** Intracellular Fl-Bgt staining of PC12 cells together with anti-Ric-3 and anti-PDI (ER marker) Ab staining. Scale bars, 5 μm.

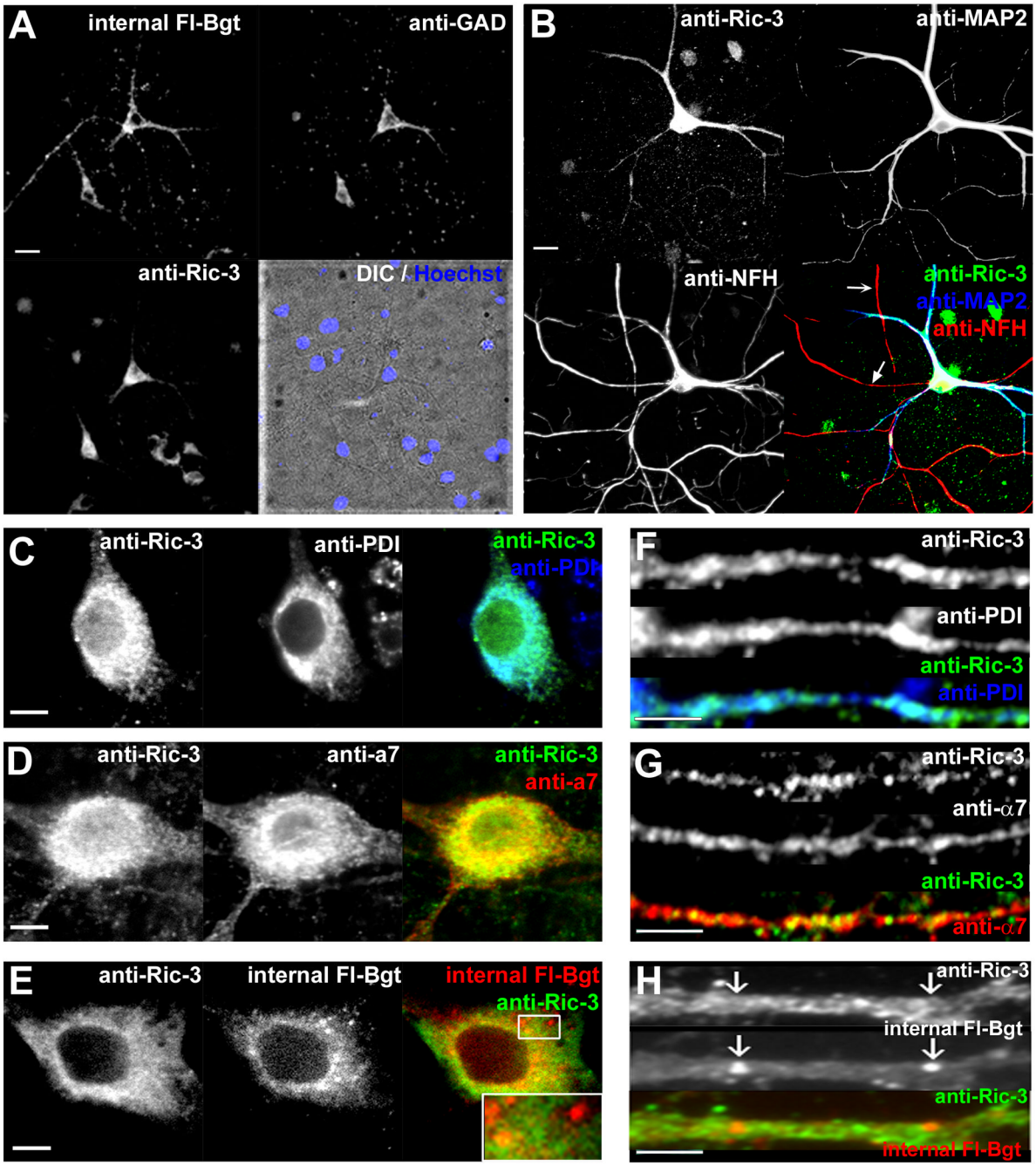

Figure 7. Native Ric-3 and α7 subunits in hippocampal neurons

Cultured hippocampal neurons (18 to 24 days in-vitro) were stained to examine the distribution of Ric-3, α7 subunits, Bgt binding sites, and ER structures. **(A)** Cultured neurons were stained with Fl-Bgt to internal sites (upper left), anti-GAD Ab (upper right) and anti-Ric-3 Ab (lower left). Stained nuclei are overlaid with a DIC image in the lower right panel. **(B)** Cultured neurons were stained with anti-Ric-3 Ab (upper left), anti-MAP2 Ab (upper right) and anti-neurofilament heavy chain (NFH) Ab (lower left). The merged image is in the lower right panel. **(C)** Somata were stained with anti-Ric-3 Ab (left) and the ER marker (anti-PDI Ab; middle). The merged image is in the right panel. **(D)** Somata were stained with anti-Ric-3 Ab (left) and anti-α7 Ab (middle). The merged image is in the right panel. **(E)** Somata stained with

anti-Ric-3 Ab (left) and stained with Fl-Bgt to internal sites (middle). The merged image is in the right panel. Examples of bright Fl-Bgt stained puncta are highlighted in the box and magnified in the inset. **(F)** Dendrites were stained with anti-Ric-3 Ab (top) and the ER marker (anti-PDI Ab; middle). The merged image is in the bottom panel. **(G)** Dendrites were stained with anti-Ric-3 Ab (top) and anti-α7 Abs (middle). The merged image is in the bottom panel. **(H)** Dendrites were stained with anti-Ric-3 Ab (top) and with Fl-Bgt to internal sites (middle). The merged image is in the bottom panel. Scale bars, 50 μm (A, B) and 5 μm (C–E, G–I).

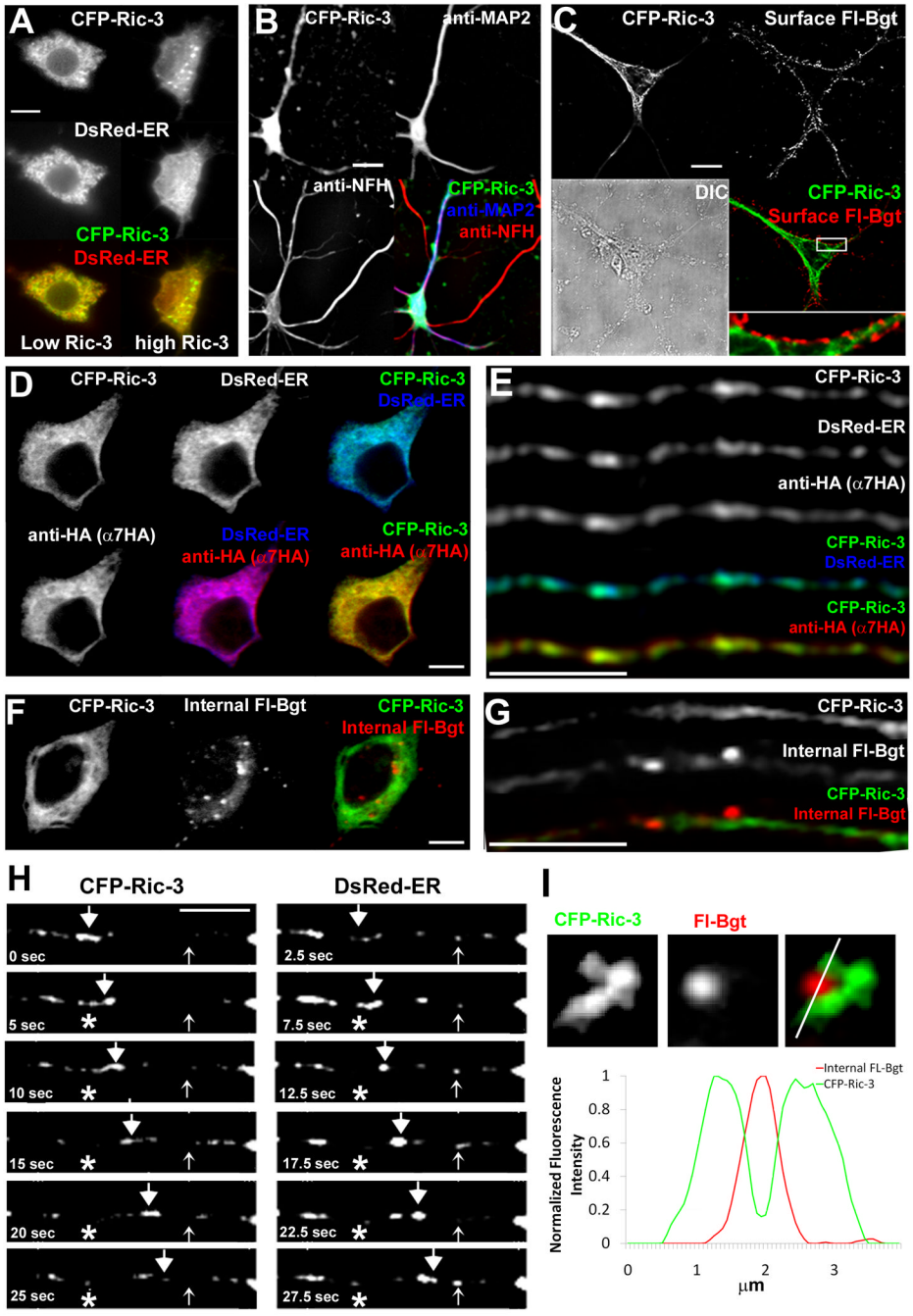

Figure 8. Transfected Ric-3 and α7 subunits in hippocampal neurons

Cultured hippocampal neurons transfected with the CFP-Ric-3, DsRed-ER, and epitope-tagged α7 constructs. **(A)** Somata imaged for CFP-Ric-3 (top) and the ER marker, DsRed-ER (middle). The merged image is in the bottom panel. On the left of each panel is a soma transfected with low levels of CFP-Ric-3 and on the right with high levels of CFP-Ric-3. **(B)** Transfected neurons imaged for CFP-Ric-3 (upper left), anti-MAP2 Ab (upper right) and anti-NFH Ab (lower left). The merged image is in the lower right panel. Image contrast has been enhanced to show distribution of CFP-Ric-3 in dendrites, which results in over-exposed somata. **(C)** Transfected neurons imaged for CFP-Ric-3 (upper left) and surface FL-Bgt (upper right). The merged image is in the lower right and the DIC image in lower left panel. **(D)** A soma from a

transfected neuron imaged for CFP-Ric-3 (upper left), DsRed-ER (upper middle) and α7-HA subunits (lower left). The corresponding merged images are in the upper right, lower middle and lower right panels as indicated. **(E)** A dendrite from a transfected neuron imaged for CFP-Ric-3 (top), DsRed-ER (2nd from top) and α7-HA subunits (middle). Merged images are in the two bottom panels as indicated. **(F)** A soma from a transfected neuron imaged for CFP-Ric-3 (left) and internal Fl-Bgt (middle). DsRed-ER (upper middle) and α7-HA subunits (lower left). The merged image is in the right panel. **(G)** A dendrite from a transfected neuron imaged for CFP-Ric-3 (top) and internal Fl-Bgt (middle). The merged image is in the bottom panel. **(H)** Time lapse images of CFP-Ric-3 and ER-DsRed transfected neurons showing an example of a fast moving puncta (large arrow heads) and static structures (small arrow heads) that contain both CFP-Ric-3 and ER-DsRed. The asterisk denotes the start location of the moving puncta. Images acquired alternated between the CFP channel and the DsRed channel with 2.5 seconds between acquisitions, starting with CFP-Ric-3 at time 0. **(I) Top:** An example of an ER sub-compartment structure imaged with CFP-Ric-3 (right) and a bright internal Fl-Bgt stained puncta (middle) in a dendrite. The merged image is in the right panel. **Top:** A line profile analysis of the Fl-Bgt (red) and CFP-Ric-3 (green) structures illustrating the Fl-Bgt puncta juxtaposed to the CFP-Ric-3 structure. Scale bars, 10 μm (A–C) and 5 μm (D–H).

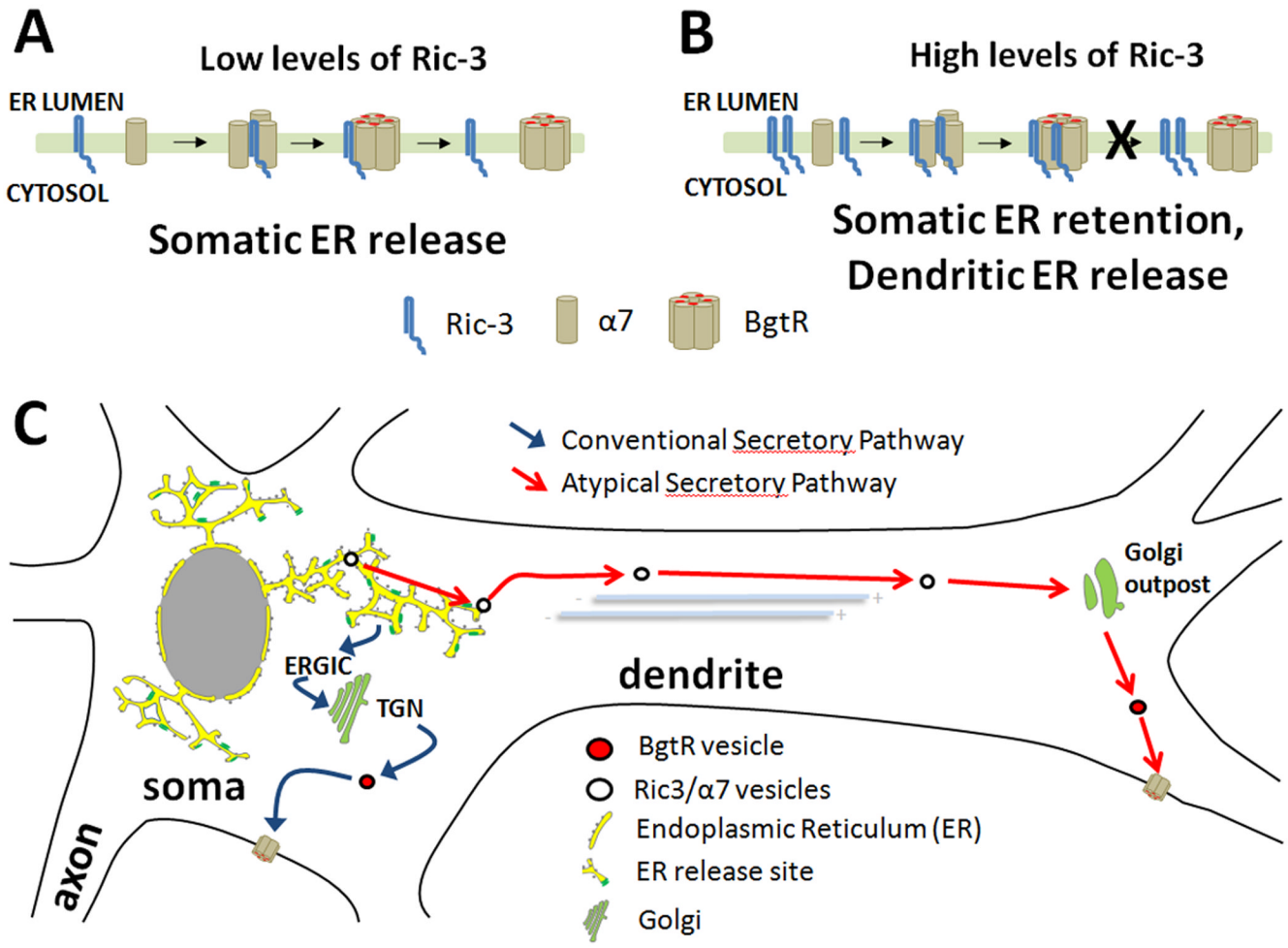

Figure 9. Model of how Ric-3 function is altered by changes in Ric-3 levels in neurons

(A) At low levels, Ric-3 interactions with α7 subunits are short-lived and mediate BgtR assembly and release from the ER. **(B)** At higher levels, Ric-3 interactions with α7 subunits are long-lived and retain BgtRs in the ER in addition to promoting BgtR assembly. **(C)** The BgtR trafficking pathway is determined by the type of Ric-3 interaction with α7 subunits. At low levels, short-lived interactions with Ric-3 result in ER release of BgtRs in the soma and BgtRs traffic through the conventional secretory pathway through the ERGIC compartment and Golgi apparatus in the soma to the plasma membrane (blue arrow pathway). At high levels, long-lived interactions with Ric-3 result in ER retention of BgtRs in the soma and BgtRs traffic through the atypical secretory pathway in transport vesicles that are part of the the ER sub-compartment in dendrites to Golgi outposts and then to the plasma membrane in dendrites (red arrow pathway).

Table 1

Distribution of Ric-3, α7 and GAD in cultured hippocampal neurons

Ab epitope	Anti-GAD	Anti-Ric-3	Anti-α7
% of total neurons	12 ± 2% (1279 neurons)	17 ± 0.7% (1129 neurons)	16 ± 1% (833 neurons)
% of GAD+ neurons	100%	92 ± 3% (126 neurons)	90 ± 8% (89 neurons)
% of Ric-3+ neurons	84 ± 3% (140 neurons)	100%	92 ± 5% (87 neurons)
% of α7+ neurons	79 ± 6% (107 neurons)	97 ± 2% (81 neurons)	100%

n=3 experiments